X-ray creation and activation of electron spin resonance in vitreous silica

F. L. Galeener, D. B. Kerwin, and A. J. Miller
Department of Physics, Colorado State University, Fort Collins, Colorado 80523

J. C. Mikkelsen, Jr.
Xerox Palo Alto Research Center, Palo Alto, California 94304

(Received 19 May 1992; revised manuscript received 24 September 1992)

We report strong dependencies of electron-spin-resonance (ESR) signals in fused silica on x-ray dose, sample hydroxyl concentration [OH], and preirradiation sample-annealing temperature T_F. In general, the strengths of the E'-center ESR signal and the two oxgyen-hole-center signals increase nonlinearly with Cu-target x-ray dose; we ascribe this behavior to the coexistence of two processes: (1) The x-ray *activation of the spins of pre-existing structural defects,* and (2) the *x-ray creation of new similar defects.* From this model and the observed nonlinear dependence on dose, we obtain relative values for the number of pre-existing defects, their rate of activation by x rays, and the rate of creation of new defects. These relative values are then examined for their trends with respect to [OH] and T_F: For example, there are far more *pre-existing* E' precursor defects in "dry" Suprasil-$W1$ ([OH] <2 ppm) than in "wet" Suprasil-1 ([OH] ≈ 1200 ppm) fused silica, yet *new* E' defects are about twice as easy to create with x rays in the "wet" material. In general, we find that the relative x-radiation "hardness" of different fused silica samples is strongly dependent on dose, hydroxyl content, and thermal history. From the [OH] and T_F dependencies of spin concentrations, we conclude that none of the three spin-active defects can be identified with either of the two previously reported Raman-active defects, traditionally labeled D_1 and D_2. Moreover, we conclude that D_2 is not a strongly preferential site for formation of the spin-active defects under x irradiation, and that D_1 is unlikely to be such a site.

I. INTRODUCTION

There is an extensive literature on the observation and interpretation of electron-spin-resonance (ESR) signals in vitreous silica (v-SiO_2). This, and work on other glasses has been reviewed by Griscom[1–6] and by Wong and Angell.[7] The electronic structure of v-SiO_2 has been reviewed by Griscom[8] and by Robertson,[9] while electronic defects have been discussed by O'Reilly and Robertson[10] and by Weeks.[11] Many general properties of v-SiO_2 are discussed in the book by Doremus.[12] It is now well known that pure v-SiO_2, which has been quenched at normal rates (by furnace cooling, manual air quenching, or manual water quenching) shows no detectable ESR signal.[3] This absence of unpaired spins in "pristine" material is also true for otherwise pure material containing the ubiquitous "water" impurity. This impurity is incorporated in the form of OH units bonded to the Si atoms in the glass[12–14] and can be detected by infrared[13,14] or Raman[15–21] spectroscopy in concentrations from ~ 1 to over 1200 ppm by weight.[20] ESR signals are observed only after the pristine material is exposed to additional disturbances, including energetic neutrons,[22–25] ions[26,27] and electrons,[28–30] γ rays[31–44] and x rays.[45–50] In contrast, bulk samples that are quenched extremely rapidly[2] and deposited thin films[51,52] often exhibit ESR response prior to any deliberate irradiation.

Three distinct ESR lines are seen at room temperature: the electronlike E' line and two holelike lines, which we call the H_W and H_D lines.

The E' line was first reported by Weeks[22] who observed a narrow absorption line with $g=2.0013$, after ^{60}Co γ irradiation. Feigl, Fowler, and Yip[53] have ascribed the E' line to the unpaired spin of an electron trapped on the unbonded sp^3 hybrid orbital of a three-bonded silicon atom at one side of an asymmetric oxygen vacancy. Their defect structure is depicted in Fig. 1(a) and we call it an asymmetric oxygen vacancy electron center (AOVEC). It is asymmetric because it includes relaxation of the second Si atom towards the plane of its three neighboring O atoms.[53] It is likely[49] that a similar E' signal will be seen at room temperature from an electron trapped on a three-bonded silicon atom that is *not* part of an oxygen vacancy, but stands "alone"—like the

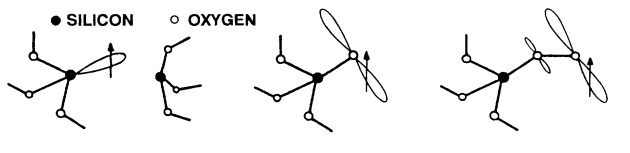

(a) ASYMMETRIC OXYGEN-VACANCY ELECTRON CENTER (AOVEC)
(b) NONBRIDGING OXYGEN-HOLE CENTER (NBOHC)
(c) PEROXYL RADICAL OXYGEN-HOLE CENTER (PROHC)

FIG. 1. Spin-active defect structures in v-SiO_2. Each ↑ represents the unpaired spin of a charge trapped near the atom shown. These structures have been assigned (Refs. 53, 39, and 25) to the E' (a), H_W (b), and H_D (c) ESR lines.

left half of the structure in Fig. 1(a). We call the "stand-alone" structure the three-bonded silicon electron center (TBSEC). Should the sp^3 orbital lose its electron, or capture another, there will be no net spin at the site, and no E' signal.

The H_W line is seen clearly in Suprasil-1,[54] a so-called "wet" material, containing high concentrations [OH] of hydroxyl units in the form $\equiv$Si-OH. H_W has been assigned by Stapelbroek *et al.*[39] to a hole trapped on the unbonded $2p$ orbital of a nonbridging oxygen atom. That structure is depicted in Fig. 1(b), and is called the nonbridging oxygen hole center (NBOHC).

The H_D line is found in Suprasil-$W1$, a "dry" material containing little or no hydroxyl, and has been attributed by Friebele *et al.*[25] to a hole trapped on the unbonded $2p$ orbital of the singly bonded oxygen atom in a dangling peroxy radical. That structure is shown in Fig. 1(c); we call it the peroxy radical oxygen hole center (PROHC).

Expanding on an earlier model by Devine and Arndt,[44] Griscom[55] has suggested that the E' and H_W spins induced by stress can be formed in *pairs* when two nearby Si-O bonds *not* on the same Si-O-Si bridge are broken and exchange an electron, leaving one positively charged defect with H_W spin and the other with a stand alone E' spin. This interesting *but unproven* model does not require an AOVEC for E' spin observation.

Except for our earlier remarks,[48] when the E' dose dependence has been reported to be nonlinear under x irradiation[48,49] or γ irradiation[40–44] this fact has either been ascribed to "recombination" of defects at high dose, or left unexplained. In this paper we show that the x-ray dose curves are generally nonlinear for all three major defects in v-SiO_2, and that data taken up to $\sim$200 Mrad (SiO_2) are fit very well by a simple piecewise linear "creation plus activation" model, not explicitly involving recombination. The resultant analysis yields a quantitative separation of creation from activation and reveals much information about these processes, the defects, their origins, and the radiation hardness of v-SiO_2.

Pure irradiated (hence no-longer pristine) v-SiO_2 generally shows at least two of the three spin signals, E', H_W, or H_D. These ESR signals can be annealed away completely by rather short exposures to fairly low temperatures; e.g., 10 min at 300 °C nearly removes the E' signal.[39] The rates for annealing away[39] the spin signals have been found to depend on OH concentration, but the dependencies have been little studied. We do not study this *annealing* process.

Rather, we present a systematic study of the ESR signals induced in v-SiO_2 by increasing doses of x radiation obtained from a Cu-target x-ray tube, preliminary results of which were reported earlier.[48,56] We sometimes observe saturation of the spin signal with dose, and always find that the induced spin signal depends on hydroxyl content and fictive temperature, as well as x-ray dose. While there is evidence that the spin-active defects giving E', H_W, and H_D spin signals are also responsible for certain optical absorption[31–34,55] and luminescence lines,[32,55] we show that they are *not* responsible for the Raman-active "defect" lines D_1 and D_2 (Ref. 16) whose origin is a topic of much recent discussion.[57–63] We also give evidence that neither D_1 nor D_2 is a highly preferential site for formation of E', H_W, or H_D spin-active defects under x irradiation.

We fit the nonlinear dose curves with a simple kinetic model involving three states of the glass network and two x-ray-induced processes that yield observable spins. The ground state of the network is "undefected" or "perfect," containing only proper Si-O bonding and *no broken bonds.* Each ESR signal is caused by a second state of the network, namely, a broken bond defect having an observable spin. We refer to defects with observable spins as "centers" or "spin-active defects." Under x-ray bombardment a center may be "created" from an undefected piece of network by permanent rupture of one or more bonds; or, it may merely be "activated" by x-ray-induced trapping or detrapping of an electron or hole on a "pre-existing" zero-spin form of the center. This second process of "activation" is presumed to cost much less energy per center (<1 eV) than the first process of "creation" ($\sim$30 eV). In the present analysis we want to emphasize that the intermediate energy spin-zero defects exist in our samples *before* irradiation, so we refer to one of them as the *pre-existing* form of the center, *pre-existing* precursor defect, *pre-existing* center precursor or simply *pre-existing* defect. For example, the terms pre-existing E'-center precursor, pre-existing E' precursor defect, and pre-existing E' defect all refer to the same state of the network: the spin-zero defect structure, which is converted under x irradiation into a spin-active E' center.

II. EXPERIMENTAL DETAILS

A. The samples

Our samples of v-SiO_2 were rectangular parallelepipeds of Suprasil-1 and Suprasil-$W1$ 3 mm$\times$6 mm$\times$0.9 mm thick, cut and polished from larger samples obtained from Heraeus-Amersil Corporation.[54] One 3-mm edge was beveled so that sample orientation could always be determined. The low hydroxyl content material, called Suprasil-$W1$, has OH concentration less than 2 ppm by weight and is very slightly oxygen rich.[64] It is traditional to refer to this material as dry. The high hydroxyl content material, called Suprasil-1, has OH concentration approximately 1200 ppm by weight. This material is commonly referred to as wet, however, no measurable fraction of the OH units is in the form of H_2O molecules.[19] Both Suprasil materials have total metallic impurity content less than 1 ppm and contain extremely few (microscopic) bubbles. They contain Cl impurities[37,55] up to $\sim$30 ppm for Suprasil-1 and $\sim$500 ppm for Suprasil-$W1$, but our measurements are unaffected by any spin signal from the Cl. Rather complete material specifications can be obtained from the manufacturer's product catalog.[54] We did not study any other types of v-SiO_2.

The final measurements were carried out on essentially four samples, two each of Suprasil-1 and Suprasil-$W1$. Each sample was prepared by annealing at a fixed tem-

TABLE I. Essential properties of the four types of v-SiO_2 samples used in this study. The samples were annealed for a sufficiently long time to come to an equilibrated structure, then air quenched rapidly, so that the annealing temperature approximates the fictive temperature T_F of the final material. This paper shows that the number of pre-existing precursor defects as well as the rate of x-ray production of similar spin-active defects both depend on T_F and hydroxyl concentration [OH].

Material "type"	Impurities >1 ppm (by weight)	Sample type	Annealing temperature T_F (°C)	Annealing time (h)
Suprasil-1	[OH]~1200 ppm	1	1350	1
"wet"	[Cl]~30 ppm	2	700	1000
Suprasil-$W1$	[OH]<2 ppm	3	1350	10
"dry"	[Cl]~500 ppm Dissolved O_2	4	1000	100

perature for a length of time known to give an equilibrated structure, as indicated by Raman studies,[65–67] and then it was air quenched to room temperature. The annealing temperatures and times are listed in Table I. The annealed samples showed no strain under crossed polarizers, gave the expected polarized Raman spectra[68–70] and showed no E', H_W, or H_D ESR signals in their pristine form.

B. X-ray exposures

Each sample was exposed to x radiation for an initial period of 1–16 h, and then its ESR signals were measured, as will be described shortly. The sample was then further exposed for a few more hours, the ESR signals remeasured, and so on, until the total x-ray exposure time was the order of 100 h. In this way ESR spectra were obtained as a function of increasing exposure on a single otherwise unperturbed sample.

The x-ray exposures were made at a constant distance of 10 cm from the external beryllium window of a GE Model CA-7 (7 kW) Cu-target tube, which was part of a GE Model 5000105G1 diffraction spectrometer. The tube was operated at 40 kV and exhibited a typical Cu-target spectrum[71] with $h\nu$ from about 3–40 keV. The total x-ray flux was monitored and kept constant from exposure to exposure. A special fixture enabled the sample to be placed in exactly the same position and orientation each time, with a particular broad surface (the "front" surface) always facing the x-ray tube and normal to the direction of the primary flux.

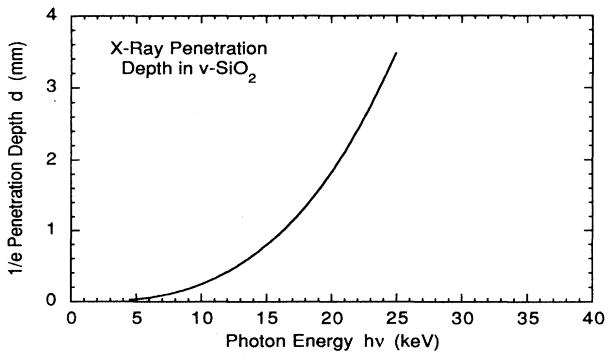

FIG. 2. The $1/e$ x-ray-absorption depth d_0 vs x-ray photon energy $h\nu$, calculated for v-SiO_2.

This latter precaution is necessary because much of the effective tube flux is absorbed near the surface where it enters the sample. This can be anticipated from Fig. 2, which shows the $1/e$ x-ray-absorption depth d_0 for v-SiO_2 versus x-ray energy. For each photon energy $h\nu$, the x-ray intensity at depth d is given by $I(d)=I_0e^{-d/d_0}$, where I_0 is the incident intensity at $d=0$, and $d_0(\text{mm})=10^4/\eta\sigma$,

$$\eta\sigma=N_A\rho(SiO_2)10^{-24}\times[\sigma(Si)+2\sigma(O)]/[A(Si)+2A(O)],$$

$N_A=6.023\times10^{23}$ atoms/mol, $\rho(SiO_2)=2.19$ g/cm^3, $A(Si)=28.1$ g/mol, and $A(O)=16$ g/mol, while $\sigma(Si)$ and $\sigma(O)$ are the total x-ray cross sections (in cm^2/g) given in Ref. 72. Figure 2 shows that most of the flux below approximately 16 keV will be absorbed in a 1-mm-thick sample, while most of that above 16 keV will be transmitted. The $1/e$ absorption depth at the Cu-K_α source peak (~8 keV) is $d_0\approx125$ μm.

The x-ray tube flux as a function of energy was calculated in two steps for the particular operating conditions and geometry of the tube used. The broadband bremsstrahlung contribution to the x-ray flux was calculated using the Kirkpatrick and Wiedmann[73] cross sections in a semiempirical algorithm developed by Birch and Marshall.[74] The intensities of the characteristic lines were calculated using the technique of Brown and Gilfrich,[75] which employs the same cross sections mentioned above, and the fluorescence yields published by Fink *et al.*[76] Corrections for absorption in the x-ray tube anode as well as absorption in the tube window and air path to the sample were included. It should be noted that there are more precise numerical methods for calculating x-ray tube output, such as the electron diffusion model of Brown and co-workers.[77,78] However, the above method is thought to yield relative values of tube flux accurate to about 15% and an absolute integrated tube intensity value accurate to about 50%. These were deemed adequate for the present work.

Figure 3 shows the calculated spectral distribution of

TABLE II. Experimental calibration factors.

(A) Incident x-ray power and dose related to exposure time t	
Total incident power density	1.84 joules cm^{-2} per h of t
Dose rate (total front surface)	2.55 Mrad (SiO_2) per h of t
Dose rate (total front surface)	4.59 Mrad (Si) per h of t
(B) Total number of spins related to ESR signal strength S	
Total number of E' spins	5.6×10^{15} per unit of $S(E')$
Total number of H_W spins	1.1×10^{6} per unit of $S(H_W)$
Total number of H_D spins	5.5×10^{15} per unit of $S(H_D)$

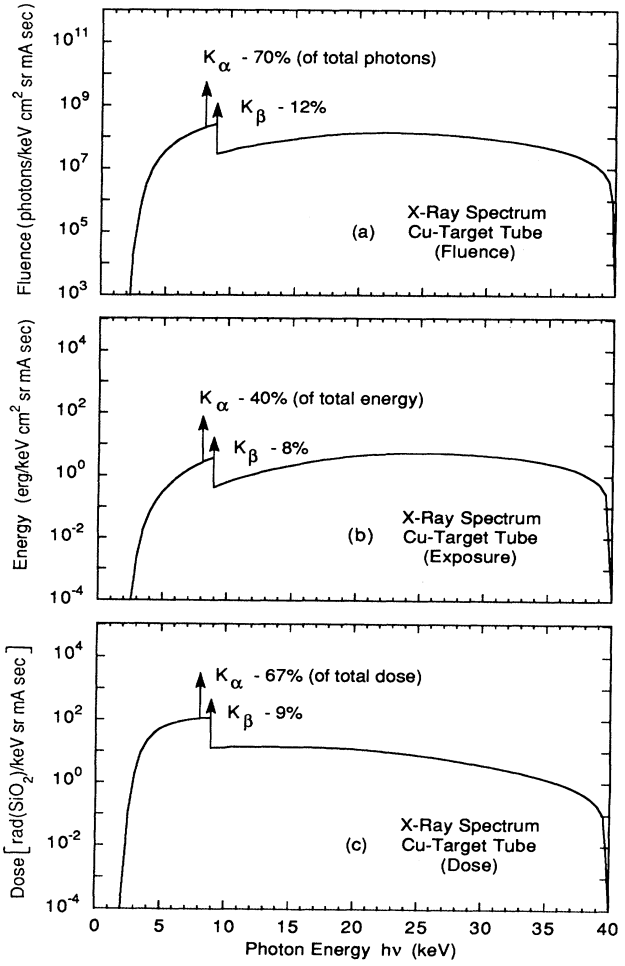

FIG. 3. The calculated spectral distribution (per steradian-milliamp-second) for x rays from the Cu-target x-ray tube operated at 40 kV: (a) fluence in photons/keV cm^2, (b) energy in ergs/keV cm^2, and (c) dose in rad (SiO_2)/keV. The Cu K_α and K_β characteristic emission lines are represented by δ fns (vertical lines) each containing the indicated percent of the area under the complete emission spectrum.

flux (per keV, per milliamp of tube current, per steradian, per second) for (a) fluence in photons/cm^2, (b) energy in ergs/cm^2, and (c) dose in rad (SiO_2). Although the natural half-widths of the Cu-K_α and Cu-K_β characteristic lines are on the order of a few eV, these lines are conveniently represented by δ functions having the following percentages of the calculated total tube flux, respectively: (a) 70 and 12%, (b) 40 and 8%, and (c) 67 and 9%.

For comparison purposes, the calculated dose rate at the front surface of the samples was 2.55 Mrad (SiO_2)/h. This dose rate decays into the sample with the absorption lengths of the various photon energies, given in Fig. 2, weighted by the relative intensities in the spectral distribution given in Fig. 3. Essentially all of the characteristic radiation is absorbed, while a significant portion of the bremsstrahlung radiation passes through the sample without interacting with the SiO_2. The dose rate at the back surface of the sample (due entirely to the bremsstrahlung) was calculated to be 76.5 krad (SiO_2)/h, about 3% of the incident dose rate.

Thus, each hour of exposure in this work corresponds to 2.55 Mrad (SiO_2) total dose at the front surface of the sample (with tube flux spectrally distributed as shown in Fig. 3, and uncertainties as stated earlier in this section). Additional exposure calibration data is given in Table II(A), where it will be seen that dose (Si) $\simeq$ 1.9 dose (SiO_2).

C. ESR spectroscopy

The ESR measurements were made at room temperature with a standard VARIAN Model E-109E spectrometer, using a TE_{102} cavity mode. The nominal operating frequency was 9.1 GHz and the cavity dimensions were approximately 10.2 mm$\times$22 mm$\times$43 mm. The sample was placed at the center of the cavity with its 6-mm length parallel to the 22-mm-cavity dimension and its 3-mm-width parallel to the 10.2-mm dimension. The sample was suspended in a fused quartz "bucket" at the end of a fused quartz rod. The holder had been flame polished and annealed and showed no spin signals of its own. This setup resulted in minimal cavity loading.

A typical E' spectrum obtained from an x-irradiated hydroxyl-containing sample is shown in Fig. 4. As indi-

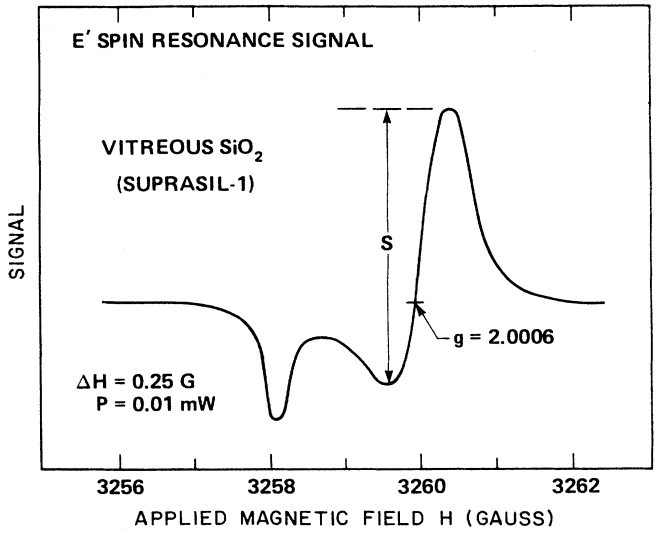

FIG. 4. A typical E' spin-resonance signal for the center shown in Fig. 1(a) as observed in this study, showing the modulation field ΔH and the microwave power level P always employed. The operating frequency in all measurements was near 9.1 GHz, and the power well below the microwave saturation level of the E' signal. The single g value is shown as a fiducial, and marks the zero crossing of the data. The strength S of the E' signals was measured as shown.

cated earlier, this ESR line is widely agreed to be the signature of an electron trapped in a dangling sp^3 orbital on a Si atom:[79,53] It is therefore a measure of the number of Si atoms that are bonded at nearly tetrahedral angles to only three oxygen atoms in the glass network, symbolized by $\equiv Si^{\bullet}$, where $\bullet$ denotes an unpaired spin. All our measurements of the E'-spin signal were made using the microwave power level P and the modulation field ΔH given in Fig. 4. These conditions preserved resolution and avoided microwave power saturation of the signal, thus ensuring that the signal strength changed linearly with the number of unpaired spins.[80] The nominal g value given in Fig. 4 corresponds to earlier observations,[23] but is not fully meaningful: The E' line is more properly interpreted in terms of the three principal values of a g tensor, that has been averaged over all solid angle orientations and over site-to-site variations in the principal axis components of the tensor, as elaborated by Griscom.[36] The value given marks the zero crossing of the derivative spectrum and is calculated from the relationship

$$g = 7.1433 \times 10^{-7} \nu H^{-1} , \quad (1)$$

where ν is the microwave frequency in Hertz (9.1274 GHz in the experiment of Fig. 4) and H is the dc magnetic field in Gauss. It has been shown by computer simulation that such zero crossings correspond approximately to g_2, the principal axis g value intermediate between the maximum and minimum values.[1] Because the nominal g value and line widths of this electron center did not vary during all our measurements, we were able to represent the E' signal strength with a single parameter S, shown as the "peak height" in Fig. 4.

Measurements of the hole center ESR signals are a little more complicated, partly because there are two types having similar signatures,[38] one predominating in wet v-SiO_2 and the other in dry material. Stapelbroek *et al.*[39] showed that in wet samples with OH $\simeq$ 1000 ppm, the dominant hole center comprises a hole trapped in a $2p$ orbital of a single (nonbridging) oxygen atom, attached to one Si atom and symbolized by $\equiv$Si-O$^{\bullet}$. We use "H_W" to label the dominant holelike spin signal in wet material, and assume with Stapelbroek *et al.*[39] that it represents a singly coordinated O atom in a NBOHC like that shown in Fig. 1(b). Friebele *et al.*[25] used ^{17}O-enriched v-SiO_2 to show that in dry samples with OH $\leq$ 10 ppm, the hole center comprises a superoxide ion O_2^- that is attached to a Si atom. This is called a peroxy radical[81] and symbolized by $\equiv$Si-O-O$^{\bullet}$. More precisely, these authors[25] find that the spin is 75% in a $2p$ orbital of the distal oxygen and 25% in the corresponding $2p$ orbital of the oxygen proximal to silicon. We use "H_D" to label the dominant holelike spin signal in dry v-SiO_2, and assume with Friebele *et al.*[25] that it represents a PROHC like that shown in Fig. 1(c).

A typical H_D spectrum obtained from an irradiated dry sample is shown in Fig. 5. The broad H_D hole center line between 3230 and about 3260 G is similar to that reported by others.[38] Note the much larger power level P, in comparison with Fig. 4. The sharper feature just above 3260 G is the E' line, which is now microwave power saturated (and therefore distorted).[94] Again the

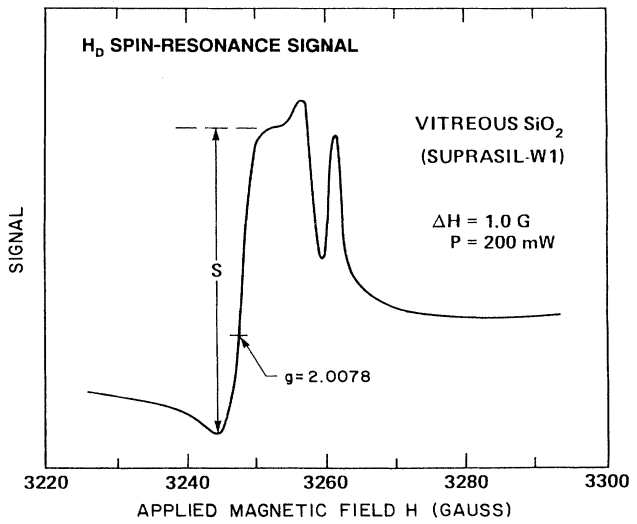

FIG. 5. A typical H_D spin-resonance signal for the NBOHC center shown in Fig. 1(b) as observed in "dry" samples in this study. We refer to this as the H_D signal to distinguish it from the slightly different H_W signal seen in the "wet" material. The modulation field ΔH and microwave power level P shown were used for all H_D and H_W measurements, i.e., on both dry and wet samples. The strength S of the hole-center signals was measured as shown, ignoring the saturated form of the E' line seen at about 3260 G in this example. The g value shown marks the zero crossing.

nominal g factor shown marks the zero crossing (hence g_2) of the H_D line. This H_D line did not change position or width in our various measurements on dry material, so we represent the H_D line strength with the single parameter S, shown as the peak height in Fig. 5.

In wet material, the hole center spectrum looked similar to that shown in Fig. 5, but was slightly wider and the zero crossing corresponded to a slightly larger nominal g factor, i.e., occurred at a slightly lower H field for the same operating frequency. The position and linewidth of this second kind of hole center (H_W) did not vary in our various measurements on wet material, so we represent the H_W line strength with its peak height S, essentially as shown in Fig. 5. Although the analysis to be presented in this paper requires only relative spin count for a given defect versus dose, the following conversion factors are given to relate the "arbitrary" spin signal, S, to an absolute number of spins (as determined by comparison of the spin signal of an appropriate sample with that of a "strong pitch" reference). The absolute calibration of the number of spins is uncertain by as much as 50% due to the manufacturer's uncertainty in the spin count of the strong pitch. For E' graphs, 1 unit of S corresponds to 5.6×10^{15} spins; for H_W graphs, 1 unit of S corresponds to 1.1×10^{16} spins; and for H_D graphs, 1 unit of S corresponds to 5.5×10^{15}. These calibration factors are compiled in Table II(B). They are quite good relative to one another, but may differ from reality by a common factor of 1 ± 0.5 (i.e., the aforementioned 50%).

III. EXPERIMENTAL RESULTS

A. Spin signal versus x-ray exposure

First consider the raw measurements of spin signal strength S versus x-ray exposure time t, obtained by the procedure described in Sec. II B. We will later convert the presentation to total spin count N versus x-ray dose D, both of which may contain scale calibration errors of $\pm50\%$, as described in Secs. II B and II C.

Figure 6 shows that in wet material the variation of E' strength versus t appears to be linear. The vertical error bars on all data points are estimates of the uncertainty in determining S from the observed spectra, and are based on multiple measurements of spectra in a few representative cases (for each sample and type of spin signal). Since there are no spin signals in the pristine materials, the points at $t=0$ are at $S=0$ and have no error bars. The tube flux was held quite constant and time was measured to 1 s, so that the horizontal error bars on the data are negligible and therefore not shown. The material that was annealed to equilibrium at $T_F=700\,^\circ$C is more E' "radiation hard" (rad-hard), since fewer E' spins are produced by a given x-ray dose than for the material with $T_F=1350\,^\circ$C. There is no hint of nonlinearity or saturation of the E' signal at the higher doses in this wet material. Full saturation would be indicated by a horizontal data curve, meaning that no further spins can be induced by additional x-ray exposure.

Figure 7 shows that for dry material the E' line strength increases monotonically with t in a way that appears to be nonlinear below about 20 h, and linear above that. In addition, the data at low exposures (below 4 h) appears to approach zero linearly. Again, the dry material annealed at a lower temperature T_F is more E' rad-hard.

Thus, the strengths of the E' signal are linear for all exposure times in wet material; while they are, respectively, linear, nonlinear, and linear at low, intermediate, and high exposure times in dry material. In both cases, significantly fewer spins are observed in material prepared with lower fictive temperature T_F, and the total spin count increases linearly at both low and high, but not necessarily intermediate, exposure times.

Figure 8 shows that for wet material the H_W line strength S increases monotonically and nonlinearly with t. The curvature appears to be less at high dose and it would appear possible to fit a linear dependence for $t>32$ h. The $T_F=700\,^\circ$C sample has nearly saturated for $t\geq32$ h. Approximately half as many H_W spins are produced in the wet material with $T_F=700\,^\circ$C, when compared with that having $T_F=1350\,^\circ$C.

Finally, Fig. 9 shows that for dry material the holelike H_D signal strength S varies even more nonlinearly with t. It appears to saturate for $t\geq32$ h. The material with

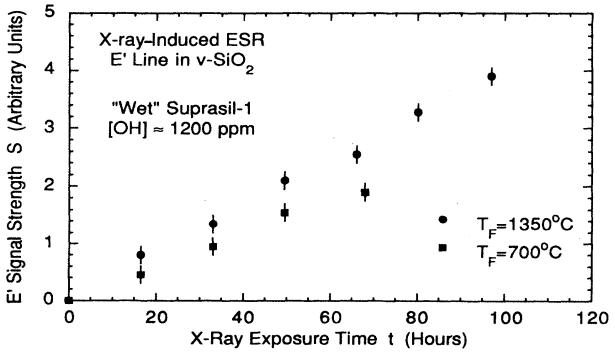

FIG. 6. The strength of the E' spin signal as a function of x-ray dose for two samples of wet Suprasil-1 vitreous SiO_2, each having a different fictive temperature T_F.

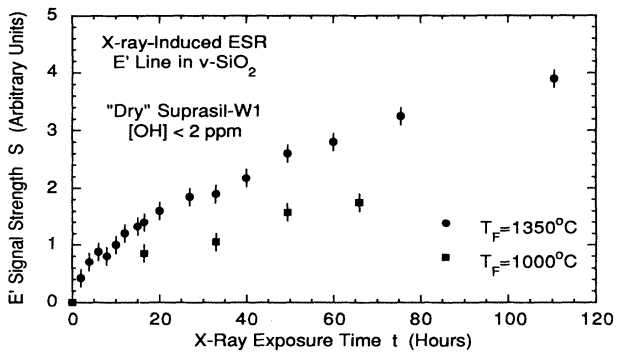

FIG. 7. The strength of the E' spin signal as a function of x-ray dose for two samples of dry Suprasil-$W1$ vitreous SiO_2, each having a different fictive temperature T_F.

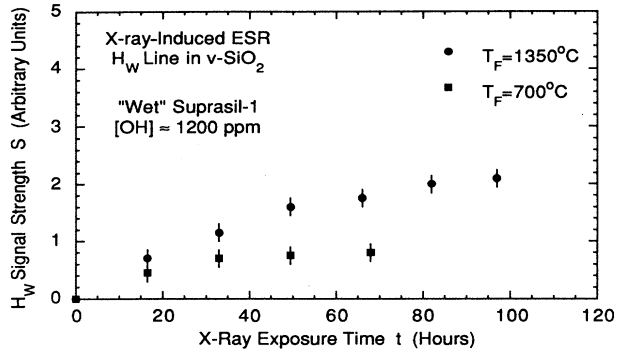

FIG. 8. The strength of the oxygen-related hole center H_W as a function of x-ray dose for two samples of wet Suprasil-1 vitreous SiO_2, each having a different fictive temperature T_F.

lower T_F shows fewer H_D spins for a given x-ray dose than does the material with higher T_F.

Thus, the strengths of the H_W and H_D signals are quite nonlinear with t at low doses, but might be represented as linear at higher doses. There is insufficient data to say whether or not S approaches zero linearly as t approaches zero. In both the wet (H_W) and dry (H_D) cases, significantly fewer spins are observed in material with lower fictive temperature. These trends for the H signals are almost the same as those seen for the E' signals, suggesting a common "model" for all four cases.

B. Spin signal versus depth into the sample

A typical experimentally measured distribution of spins is shown in Fig. 10, where the dashed line is intended to guide the eye, and enable extraction of some simple parameters. These results were obtained as follows. We began with the dry sample that had originally been annealed at $T_F=1350\,°C$ (Sample 3 in Table I) and had subsequently been exposed to a total of 110 h of x irradiation (as indicated in Fig. 7). The E' strength from the entire sample was remeasured and defined as $S(x=0)$. Then 43 μm of material was ground (and polished) off the front face and the E' strength of the remaining parallelepiped

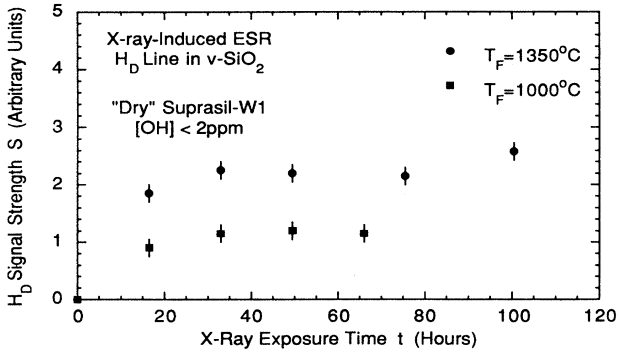

FIG. 9. The strength of the oxygen-related hole center H_D as a function of x-ray dose for two samples of dry Suprasil-$W1$ vitreous SiO_2, each having different fictive temperature T_F.

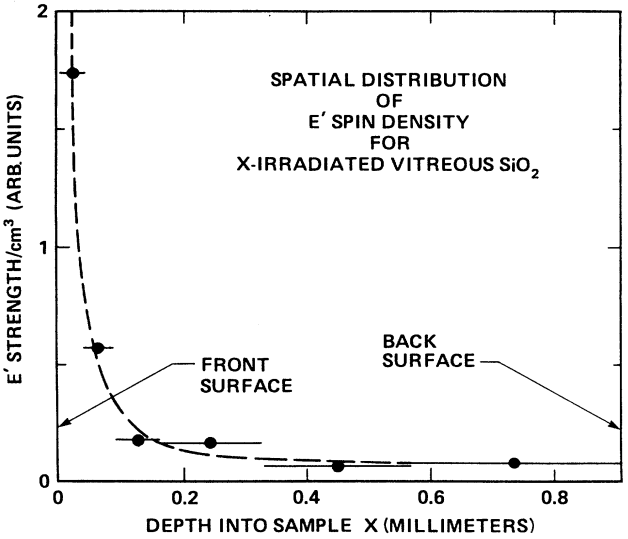

FIG. 10. A measurement of the spatial distribution of E' spin signal in the $T_F=1350\,°C$ dry sample of Fig. 7 after the total x-ray exposure time of 110 h. Note the high spin density just beneath the front surface (which faced the x-ray source) and the precipitous drop to an apparently uniform background level that extends nearly 1 mm to the back of the sample. The data was obtained by polishing away layers of the sample. From this figure, we deduced the approximate measurements of the "spin signal skin depth" Δ_S and the "background" spin density δ_B that are reported in row (2) of Table III.

was measured and defined as $S(x=43\ \mu m)$. The difference $S(x=0)-S(x=43\ \mu m)$ gave the spin signal in the first 43 μm of the original sample, and when divided by the thickness of removed material, this gave a measure of the density of spin signal, i.e., the E' strength/cm^3 plotted as the highest solid point in Fig. 10. The horizontal bar on the point runs from $x=0$ to 43 μm indicating the width and position of the thin slab of sample for which the point gives the mean spin density. We next removed an additional 44 μm of material, and by repeating the above procedure obtained the second highest point in Fig. 10, which represents the mean E' spin density in the slab from $x=43\ \mu m$ to $x=87\ \mu m$. Because the spin density was dropping rapidly we removed thicker slabs as the procedure went on. Unfortunately, this method destroys the sample.

The data in Fig. 10 show clearly that the spin density decreases very rapidly beneath the front surface, but drops to an apparently spatially uniform "background" value, rather than to zero. We estimate this background spin density level to be $\delta_B=0.16\pm0.02$ in the units of Fig. 10, which are proportional to E' spin signal/cm^3. The rate at which the high front surface density drops toward the background value is measured by the "spin signal skin depth," Δ_S, at which depth the density has dropped halfway from the highest measured value towards the background value: We estimate from the original data that $\Delta_S=33\pm10\ \mu m$. The parameters δ_B, Δ_S, and other information about the sample involved in Fig. 10 are listed in the second row of Table III.

TABLE III. The spatial distribution of x-ray-induced spin signals in three samples, for different circumstances of defect type and OH concentration. The samples corresponding to the maximum exposure times and the $T_F = 1350\,^{\circ}C$ curves in Figs. 6, 7, and 9 were sectioned, as exemplified in Fig. 10, to determine the "uniformly distributed" background spin density δ_B, and the "skin depth" Δ_S of the spins whose density rapidly decreases beneath the front surface. The trends in δ_B and Δ_S are discussed in Secs. III B and VII.

Row	ESR signal	Nominal OH content	T_F (°C)	x-ray exposure (h)	Reference Fig.	Background spin density δ_B (units of S)	Spin skin depth Δ_S (μm)
(1)	E'	1200 ppm	1350	96	6	0±0.02	40±15
(2)	E'	<2 ppm	1350	110	7	0.16±0.02	33±10
(3)	H_D	<2 ppm	1350	100	9	0.22±0.04	38±10

Similar measurements were made on the H_D line of the dry sample that had been annealed at $T_F = 1350\,^{\circ}C$ and had subsequently been exposed to 100 h of x irradiation (as indicated in Fig. 9). The background spin density was somewhat larger, $\delta_B = 0.22 \pm 0.04$, and the spin signal skin depth may be a little larger, $\Delta_S = 38 \pm 10$ μm. Information about this sample is entered in the third row of Table III.

A third sample was sacrificed to obtain spin density distribution data on the E' line in the wet sample that was annealed at $T_F = 1350\,^{\circ}C$ and subsequently exposed to 96 h of x irradiation (as indicated in Fig. 6). This material showed *no background level,* $\delta_B = 0 \pm 0.02$, and apparently had a somewhat larger spin signal skin depth, $\Delta_S = 45 \pm 15$, all listed in the first row of Table III.

Because the measurements were quite time consuming and because δ_B and Δ_B are crude measures, we carried out no more of these spin density profiles. With patience the technique could be improved to give better depth resolution. As it turns out, our choice of samples (three distinctive and strong S vs t behaviors) reveals two simple trends: As one moves down in Table III, the background level δ_B *increases* convincingly, while the spin signal skin depth Δ_B is *constant within the uncertainties.*

IV. A SIMPLE CREATION PLUS ACTIVATION MODEL FOR X-RAY INDUCTION OF SPIN RESONANCE IN v-SiO_2

We emphasize that the model to be presented next is for a single x-ray photon energy $h\nu$ and therefore must be interpreted for the present data in terms of effective rates and cross sections due to the superposition of the interactions at all of the photon energies present in the spectral distribution of the x-ray tube. This is not a serious limitation because the majority of tube output was near 8 keV as described in Sec. II B.

There are numerous hints in the data that two kinds of processes may be involved. Thus, the S vs t curves (Figs. 6–9) tend to show a linear region at low exposure times followed by a second linear region with lower slope at higher t. Also, the spin density profiles (Fig. 10 and Table III) tend to show a component that rapidly decreases below the exposed surface, as well as a second component that is distributed more uniformly through the depth of the sample. Galeener and Mikkelsen[48] first proposed that the two x-ray-induced processes are (1) the spin *activation of pre-existing structural defects by charge transfer,* and (2) *the creation of new structural defects by the rupturing of bonds.*

It is known that near-ultraviolet electromagnetic radiation can induce E- and H-spin signals in v-SiO_2,[82] at photon energies that are too small to displace an atom and thereby create a defect. It is therefore usually assumed that the low-energy photons are able to transfer electrons or holes from somewhere in the glass to a pre-existing defect and thus create an unpaired spin at the site—hence an ESR signal. This is the process of spin *activation* of a pre-existing defect. It is clear that much more energetic photons in the form of x rays should be able to do the same. The most important feature of the activation process is that spin signals produced by activation will saturate when all the pre-existing defects have been exhausted.

It is clear that the x rays involved (as well as energetic neutrons, ions, electrons, and γ rays) also have enough energy to rupture bonds and thereby create new structural defects in the material. Spin signals thus produced will increase linearly with total x-ray exposure, until the material is so riddled with defects that it becomes unstable, or until it becomes perceptibly difficult for an x ray to find a bond that has not already been ruptured. Since the present experiments look at total spin densities that are 5–7 orders of magnitude below the number density of atoms, we believe that we are far from this saturation level for the creation of defects. We assume that there is enough x-ray energy available that every defect created is also automatically activated.

Under these assumptions we write

$$N(D) = N_A(D) + N_C(D) \,, \tag{2}$$

where $N(D)$ is the total number of spins of a given type (say E') induced after accumulated x-ray dose D, while $N_A(D)$ is the total number induced by activation, and $N_C(D)$ is by creation. (We will later convert S versus t data to give N versus D, for comparison with the present model.)

We assume that the number of *activated* pre-existing sites will asymptotically approach N_0 according to

$$N_A(D)=N_0[1-\exp(-D/D_0)] , \quad (3)$$

where N_0 is the number of pre-existing (unactivated) defect sites of the specified type and D_0 is the dose at which a fraction $1/e$ of the pre-existing defects have been activated. This behavior with dose is shown in Fig. 11(a), where the initial fast rise is indicated by the slope

$$M_A \equiv [dN_A/dD]_{D=0}=N_0/D_0 . \quad (4)$$

N_0, D_0, and M_A are independent of D. We speak of "high dose" when saturation is nearly complete, say 98% for $D \geq 4D_0$.

For *creation* we write

$$N_C(D)=M_C D , \quad (5)$$

where M_C is independent of D, so that spin count due to newly *created* defects of the specified type increases linearly with dose. This behavior is depicted in Fig. 11(b) where the slope is M_C for all D. Since $dN_C/dD=M_C$, this is a "constant rate process."

The combined contribution of creation plus activation to spin count $N(D)$ is depicted in Fig. 11(c) as the sum of the quantities in Figs. 11(a) and 11(b), as required by Eq. (2). This is the general behavior of the data presented in Figs. 6–9. As D increases, $N(D)$ asymptotically approaches a straight line of final slope $M_F=M_C$; i.e., *above saturation ($D \geq 4D_0$) the slope of the data is the rate of creation of new defects (M_C).* Projection of the high dose straight line down to $D=0$ yields N_0; i.e., *the zero dose intercept of the straight-line behavior above saturation is the number of pre-existing defects (N_0).* The initial slope of the data at low dose ($D<D_0$) is given by $M_I \equiv M_A+M_C$, so that M_A *is calculated from the low and high dose slopes of the data by using* $M_A=M_I-M_C$. This elementary analysis enables the experimenter to quickly assess a measure of the number of pre-existing defects (N_0) and the relative rate of creation (M_C) and activation (M_A).

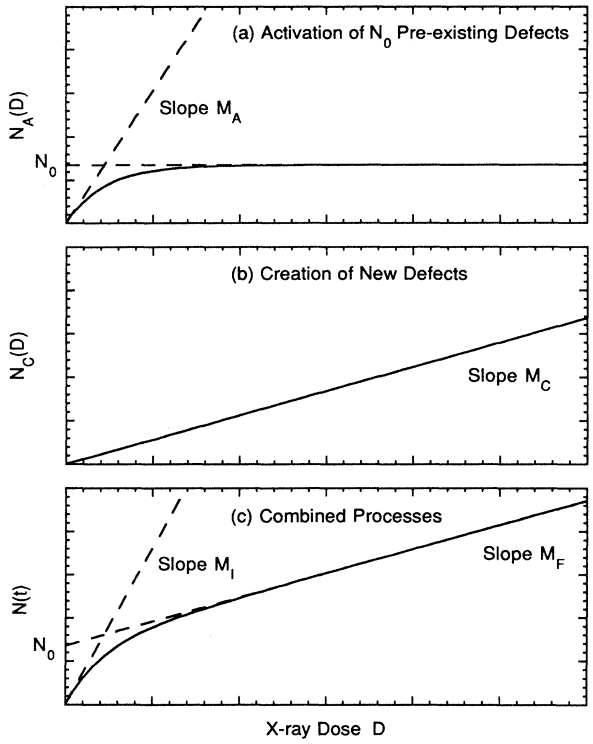

FIG. 11. A graphical representation of the creation plus activation model used to analyze the data in Figs. 6–9. The x-ray flux accomplishes two things: (a) the gradual *activation* of N_0 pre-existing precursor defects [represented by an exponential approach of $N_A(t)$ towards N_0]; and (b) the gradual *creation* of additional defects at a constant rate. The simultaneous action of these two processes (c) produces a dependence that looks very much like that measured in Figs. 6–9. Note that the linear portion of the combined process, seen at high dose, projects to the number of pre-existing precursor defects N_0, at $D=0$.

V. OTHER POSSIBLE MODELS

While the creation plus activation model is appealing in its simplicity and leads to numerous reasonable interpretations, it is not unique in its ability to fit the present data. We have found at least four ways to fit the nonlinear curves observed in Figs. 6–9, within present experimental error. On the assumption that the concentration of reaction product C, denoted $[C]$, is proportional to the spin signal, they include the following.

(1) Two parallel, irreversible reactions, *like creation plus activation,* with one of the initial reactants depletable:

$$[A] \xrightarrow{k_1} [C] ;$$

$$[B] \xrightarrow{k_2} [C] .$$

(2) A single reversible reaction with forward and backward rate constants:

$$[A] \underset{k_2}{\overset{k_1}{\rightleftarrows}} [C] .$$

(3) Two parallel reversible reactions, with B depletable:

$$[A] \rightleftarrows [C] ;$$

$$[B] \rightleftarrows [C] .$$

(4) Two consecutive reactions, the second reversible:

$$[A] \rightarrow [B] \rightleftarrows [C] .$$

Models (1) and (3) require two types of reactants, one of which is depleted, to yield saturation of the data. Models (2) and (4) require only one type of reactant (e.g., the perfect SiO_2 network), which need not be depleted to approximate the kind of saturation observed in the raw data. The data in Figs. 6–9 plus available knowledge do not allow elimination of models (2) through (4). Thus, while a good fit to the experimental data is certainly a

necessary condition for considering a kinetic model, it is not sufficient to guarantee the model's correctness.

VI. LEAST-SQUARES FITS OF CREATION PLUS ACTIVATION MODEL TO THE DATA

The raw data points for S vs t in Figs. 6–9 are replotted in Figs. 12 and 13, but now in terms of the total number of spins in the sample $N(D)$ vs x-ray dose D in Mrads (SiO_2). The conversion factors $S \rightarrow N$ and $t \rightarrow D$ are given in Table II and discussed in Secs. II B and II C. Note that Fig. 12 is for wet material (Figs. 6 and 8), while Fig. 13 is for dry (Figs. 7 and 9). All curves in Figs. 12 and 13 can be compared quantitatively *with one another* within the uncertainties in N shown by the vertical error bars and with essentially no uncertainty in D. Notice that the vertical scales for N are now identical for all measurements. As discussed in Secs. II B and II C the absolute value of the D scale common to all curves in Figs. 12 and 13 may be in error by $\pm 50\%$, and similarly for the N scale. This calibration uncertainty in D and N is relevant for comparison of the data with data taken elsewhere, but does not apply to intercomparisons within Figs. 12 and 13.

The solid lines in Figs. 12 and 13 are least-squares best fits of the data to Eqs. (2), (3), and (5). The computer determined parameters and their uncertainties are given in Table IV for all eight fitted curves. Rows (5)–(7) were the result of "blind" fits, where all three parameters N_0, M_C, and D_0 were allowed to vary. Only the data for row (5) (Fig. 13(a)—1350 °C] contains enough points below saturation to give a relatively accurate value for D_0, namely, $D_0 = 22 \pm 4$ Mrads (SiO_2). That the data for rows (6) and (7) returned $D_0 = 20$ and 18 Mrads (SiO_2), respectively (with large errors), is probably due to the lack of data points between 0 and ~ 40 Mrads (SiO_2) in all cases except for row (5) (Fig. 13(a)—1350 °C]. The average D_0 for rows (5)–(7) is $D_0 = 20$; we therefore fix D_0 at this value for all the rest of the data, rows (1)–(4) and row (8). The least-squares fit for these five rows has only two free parameters, N_0 and M_C. This procedure is slightly different than that used to construct Table I in Ref. 50, so the entries are slightly different.

The resultant errors in the M_A are large, so that as in Ref. 50 only the value $M_A = (31 \pm 6.2) \times 10^{13}$ spins per Mrad (SiO_2) for E' data on Suprasil-1 with $T_F = 1350$ °C [row (5)] is taken to be meaningful. Additional low D points were not obtained subsequently for two reasons: (1) most of the samples were destroyed in obtaining depth profiles like those described in Sec. III B and (2) a repeat of the data with more points would have required many hundreds of hours of exposure in the x-ray machine, and this time was unavailable. We, therefore, are able to make only very limited use of the derived values of M_A and/or D_0.

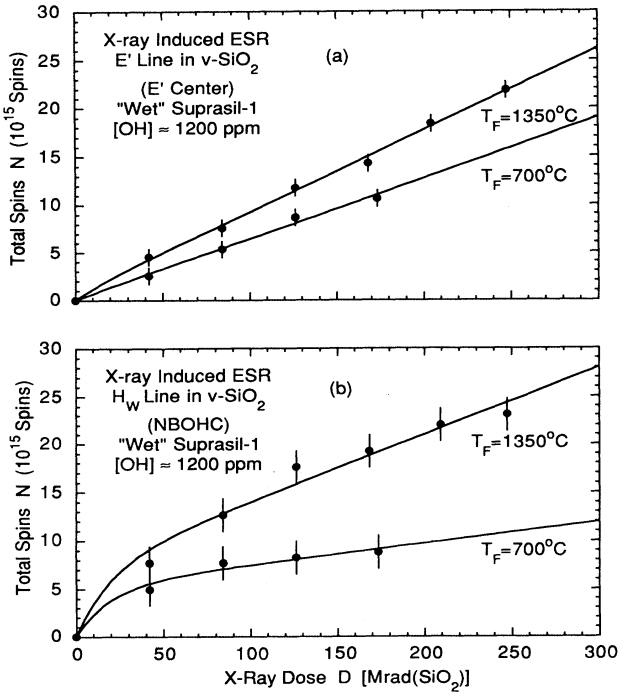

FIG. 12. The total number N of E' spins (a) and H_W spins (b) induced in wet Suprasil-1 vs total Cu-tube x-ray dose D, for two different fictive temperatures T_F. The curves are fits of the creation plus activation model [Eqs. (2)–(5) and Fig. 11] using the parameters in Table IV.

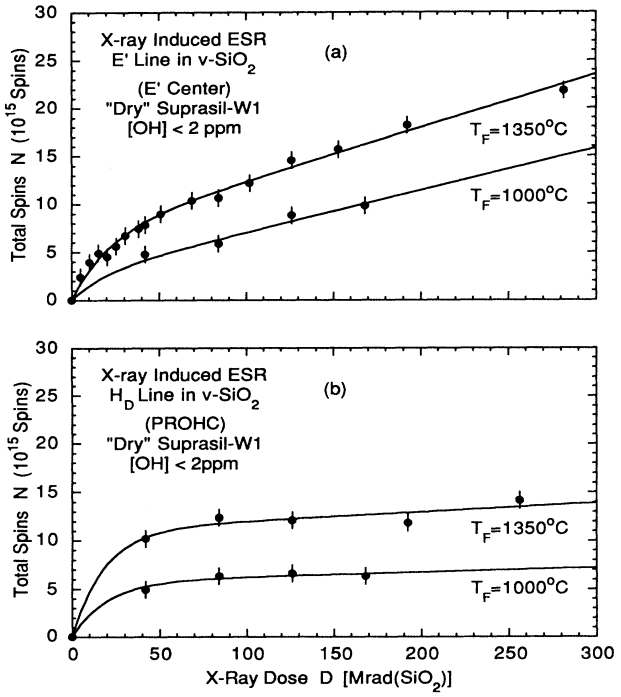

FIG. 13. The total number N of E' spins (a) and H_D spins (b) induced in dry Suprasil-$W1$ vs the Cu-tube x-ray dose D, for two different fictive temperatures T_F. The curves are fits of the creation plus activation model [Eqs. (2)–(5) and Fig. 11] using the parameters in Table IV.

TABLE IV. Parameters [sixth–eighth columns] that provide a least-squares fit of the creation plus activation model to the N vs D data, giving the solid line curves in Figs. 12 and 13. The data were fit to Eqs. (2), (3), and (5). In rows (5)–(7) the free parameters N_0, M_C, and D_0 were returned by the computer as shown. In the other rows, D_0 was restricted to 20 for reasons given in the text and the free parameters N_0 and M_C were returned as shown. The resultant $M_A = N_0/D_0$ are shown in the ninth column and are rather uncertain, except for row (5). The tenth and eleventh columns give the relative strengths of the Raman-active "defect" lines D_1 and D_2 as determined for the same materials in Ref. 67 and discussed in Sec. VIII. The numerous trends and conclusions to be drawn from this table are discussed in Secs. VII–IX. The entry in row (1) and column six is $N_0 = 0.7 \times 10^{15}$ total spins.

(1) Sample [OH]	(2) Spin type	(3) T_F (°C)	(4) Ref. Fig.	(5) Row	(6) $10^{-15}N_0$ Pre-existing	(7) $10^{-14}M_C$ (Mrad^{-1}) Creation rate	(8) D_0 (Mrad)	(9) $10^{-13}M_A$ (Mrad^{-1}) Activation rate	(10) $A(D_1)$ Raman	(11) $A(D_2)$ Raman
Suprasil-1	E'	1350	12(a)	(1)	0.7±0.4	8.5±0.3	20±0	3.5±2.0	2.4	2.8
[1200 ppm]		700	12(a)	(2)	0.1±0.6	6.3±0.5	20±0	0.5±3.0	1.2	0.4
"wet"	H_W	1350	12(b)	(3)	7.0±1.2	7.0±0.7	20±0	35±6.0	2.4	2.8
		700	12(b)	(4)	5.2±0.8	2.2±0.6	20±0	26±4.0	1.8	1.2
Suprasil-$W1$	E'	1350	13(a)	(5)	6.8±0.6	5.6±0.4	22±4	31±6.2	2.4	2.8
[<2 ppm]		1000	13(a)	(6)	2.6±2.3	4.4±1.6	20±49	13±34	1.2	0.4
"dry"	H_D	1350	13(b)	(7)	11.0±1.3	1.0±0.7	18±9	61±31	2.4	2.8
		1000	13(b)	(8)	5.7±0.4	0.5±0.4	20±0	28±2.0	1.8	1.2

VII. TRENDS IN THE PARAMETERS N_0, M_A, AND M_C

Inspection of Figs. 6–9 in terms of Fig. 11 reveals that the slope M_F of a straight line through the high dose data and the zero dose intercept N_0 of that straight line are generally well defined, but that the slope M_I of the data at low dose is reliably determined only for the $T_F = 1350$°C curve in Fig. 7 (where many points were taken at low t). It appears that $N_0 \simeq 0$ and that $M_I \simeq M_F$ for both curves in Fig. 6, i.e., for E' spins in wet Suprasil-1. These simple observations have bearing on the parameters in Table IV and the corresponding fitted curves in Figs. 12 and 13: In general N_0 and M_C ($\simeq M_F$) are reasonably well determined in Table IV, but M_A is not [except for row (5)].

A. Trends in the number of pre-existing defects

1. *Trends of N_0 with fictive temperature T_F*

Rows (5)–(8) of Table IV show that within experimental uncertainties the numbers of pre-existing E' and H_D precursor defects in dry Suprasil-$W1$ *decrease* with decreasing fictive temperature. This is as one might predict: Fewer defects would be expected when a glass is annealed to *equilibrium structure* at a lower temperature (T_F). For the latter reason, we accept as truth the appearance in rows (1)–(4) of Table IV that the numbers N_0 of pre-existing E' and H_W defects in wet Suprasil-1 also decrease with decreasing T_F (although the fit uncertainties do not firmly support this conclusion). *The data on Suprasil-1 and Suprasil-W1 thus show that the numbers of pre-existing E', H_W, and H_D center precursors are reduced when T_F is reduced.*

Additional observations on the behavior of N_D with T_F are tabulated in Table V. The fourth column shows for each case the ratio of the number of pre-existing defects at the lower temperature T_L to that at the higher temperature T_H (1350°C = 1623 K). This will be compared with the fifth and sixth columns for the Raman-active defects in Sec. VIII A.

From the changes of N_0 with T_F we can make estimates of the possible energies of thermal formation of the

TABLE V. Fictive temperature-dependent properties of the number of pre-existing defects N_0, derived from data in the indicated rows of Table IV [e.g., (1) and (2)]. T_L and T_H are the lower and higher fictive temperatures for each spin type, given in Table IV. The ratio $N_0(T_L)/N_0(T_H)$ for each precursor defect is to be compared with the ratio for the number of Raman-active "defects" in the fifth and sixth columns. The nominal energies of thermal formation E are calculated using Eq. (7) and given in the eighth column, with the error determined range indicated by minimum and maximum values given in the seventh and ninth columns. In the fifth and sixth columns, * indicates incompatibility with the entry in the fourth column while † denotes incompatibility with the seventh–ninth columns.

Rows, Table IV	(1) Sample	(2) Spin type	(3) Assigned defect structure	(4) $N_0(T_L)/N_0(T_H)$	(5) $A(T_L)/A(T_H)$ D_1	(6) $A(T_L)/A(T_H)$ D_2	(7) E (eV) Min	(8) E (eV) Nom	(9) E (eV) Max
(1) and (2)	Suprasil-1	E'	AOVEC	0.14±0.84	0.50	0.14	0.09	0.41	∞
(3) and (4)		H_W	NBOHC	0.74±0.17	0.75	0.43*†	−0.01	0.06	0.13
(5) and (6)	Suprasil-$W1$	E'	AVOEC	0.38±0.34	0.50	0.14	−0.01	0.49	1.63
(7) and (8)		H_D	PROHC	0.52±0.07	0.75*†	0.43	0.23	0.34	0.43

defects. In Ref. 67 it was shown that the concentrations of small (pre-existing) Raman-active defects D_1 or D_2 obey an Arrhenius-like relation,

$$N_D(T_F)=Ae^{-E/kT_F}, \tag{6}$$

where E is the positive energy that must be supplied to form one defect of the particular type, k is Boltzmann's constant, and T_F is the *fictive* temperature of the sample, *in kelvin*. Let us assume that this is also true for the point defects of interest here. When N_0 is known at "low" fictive temperature T_L and also at a higher one T_H, Eq. (6) results in

$$E=k\left[\frac{T_HT_L}{T_H-T_L}\right]\ln\left[\frac{N_0(T_H)}{N_0(T_L)}\right], \tag{7}$$

where use of $k=8.62\times10^{-5}$ eV/K gives E (eV).

Application of Eq. (7) to pairs of N_0 values in Table IV [e.g., those in rows (1) and (2)] yields the value of E given in Table V. Unfortunately there are large uncertainties in E for the E' precursors. Within those uncertainties, it is possible that the thermal formation energy is the same for E' precursors in wet Suprasil-1 and dry Suprasil-$W1$. The thermal formation energy for H_W (NBOHC) precursors in wet Suprasil-1 is significantly less than that for H_D (PROHC) precursors in dry Suprasil-$W1$. Further experiment is required to see if the N_0 for each defect actually exhibits Arrhenius behavior [Eq. (6)] versus T_F.

2. *Trends of N_0 with hydroxyl concentration [OH]*

It is clear from rows (1) and (5) of Table IV that for $T_F=1350$ °C there are far fewer pre-existing E' precursor defects in wet Suprasil-1 than in dry Suprasil-$W1$, by an order of magnitude or more. This is likely to be true for other fictive temperatures, since the thermal energies required for defect structure formation are expected[67] to be about the same at other T_F. The observation of fewer E' defects in wet than dry material is consistent with the structure pictured in Fig. 1(a), and the intuitive notion that the availability of large numbers of single bond-OH units in wet material would convert most of such oxygen vacancy sites from E' center precursors to pairs of *spin-inactive* ≡Si-OH sites. The observation is similarly consistent with the model of "isolated" TBSEC sites mentioned in the Introduction.

Since the H_D line is not found in Suprasil-1, it is likewise clear that there are far fewer H_D (PROHC) precursors in wet Suprasil-1 than in dry Suprasil-$W1$. Similarly, the absence of the H_W line in Suprasil-$W1$ indicates there are far fewer pre-existing H_W (NBOHC) defects in dry Suprasil-$W1$ than in wet Suprasil-1.

We have thus shown that the concentrations of pre-existing E', H_W, and H_D precursor defects all change greatly in going from Suprasil-1 to Suprasil-$W1$. This is likely associated with the dominant impurity concentration, [OH], but the present data do not rule out possible roles for increased Cl impurities or dissolved O_2 in Suprasil-$W1$ (see Table I). For example, the presence of excess oxygen in the latter case might well promote the thermal formation of large numbers of PROHC defects, showing the H_D ESR line.

B. Trends in the rate of activation of pre-existing defects, M_A

From the entries in the ninth column of Table IV it is clear that only $M_A=(31\pm6.2)\times10^{13}$ per Mrad (SiO_2) is well determined. All entries might appear to satisfy $M_A\sim30\times10^{13}$ per Mrad (SiO_2), except for rows (1) and (2), which appear to be significantly smaller. But even this simple statement is speculative because of the absence of points below ~40 Mrad [except row (5)] and the very small value of N_0 in rows (1) and (2). We really cannot infer reliable trends in M_A from our data.

C. Trends in the rate of x-ray creation of new defects, M_C

1. *Trends of M_C with fictive temperature T_F*

The seventh column of Table IV reveals that all M_C are well determined, except the values in rows (7) and (8). Rows (1)–(4) show that for E' and H_W centers in Suprasil-1, M_C decreases when T_F is decreased, within experimental uncertainties. Rows (5)–(8) suggest that for E' and H_D defects in Suprasil-$W1$, M_C also decreases with T_F, but this is not certain within the experimental errors. With the last proviso, we conclude that *for E', H_W, and H_D defects in Suprasil-1 and Suprasil-$W1$, the x-ray rate of creation of new centers M_C decreases with fictive temperature T_F.*

Additional observations on the behavior of M_C with T_F are tabulated in Table VI. The fourth column shows for each case the ratio of the x-ray rate of creation of new centers at the lower temperature T_L to that at the higher temperature T_H (1350 °C = 1623 K). This will be compared with the fifth and sixth columns for the Raman-active defects in Sec. VIII B.

Application of Eq. (7) to pairs of M_C values in Table IV [e.g., those in rows (1) and (2)] yields the values of E given in Table V. The values of E for E' and H_W centers in Suprasil-1 are well determined, those for Suprasil-$W1$ less so. For example, E for E' centers in Suprasil-1 is clearly less than for H_W centers, and probably less than E for E' and H_D centers in Suprasil-$W1$. Again, further experiment is required to see if the M_C for each spin-active defect actually exhibits Arrhenius behavior [Eq. (6)] versus T_F.

2. *Trends of M_C with hydroxyl concentration [OH]*

Comparison of the M_C in rows (1) and (5) of Table IV shows clearly that the rate of x-ray creation of new E' defect spins in material with $T_F=1350$ °C decreases going from wet Suprasil-1 to dry Suprasil-$W1$. Because OH is the dominant impurity and decreases in going from Suprasil-1 to Suprasil-$W1$ (see Table I), we ascribe the observed reduction in M_C to the decrease in [OH], although some role for increasing [Cl] and/or [O_2] is not ruled out by the present data. Our ascription is supported by the strong roles given to mobile −H or −OH units in other

discussions[1-6] of point defect formation in v-SiO_2. Further comparison of the M_C in rows (2) and (6), (3) and (7), and (4) and (8) of Table IV confirm the trend: *The rate of x-ray creation of new E', H_W, and H_D defects decreases on going from wet Suprasil-1 to dry Suprasil-$W1$, and this is presumed to be due to the decreasing hydroxyl concentration [OH].*

The very similar high dose slopes for E' and H_W spins evident in Fig. 12 shows that new E' and H_W defects are created by x rays at about the same rate in Suprasil-1 with $T_F = 1350$ °C. This near equality of the M_C [see rows (1) and (3) in Table IV] raises the possibility that x rays in wet Suprasil-1 produce new E' and H_W defects in pairs, as was noted in Ref. 50. As T_F is lowered to 700 °C, however, the near equality of M_C is lost [see rows (2) and (6) in Table IV], weakening the inference that a significant fraction of E' and H_W are formed in pairs. Comparison of rows (5) and (7) as well as (6) and (8) reveals that new E' and H_D defects are *not* created at nearly equal rates in Suprasil-$W1$. Since the E defects are always created at higher rates than the H defects, it is still possible that one component of E' defects is formed in pairs with an H defect, while an additional component is formed alone.

The nearly horizontal high dose slopes in Fig. 13(b) and the small values of M_C in rows (7) and (8) of Table IV show that *it is relatively difficult for x rays to create new H_D (PROHC) defects in Suprasil-$W1$.* Since Suprasil-$W1$ contains relatively large numbers of pre-existing PROHC precursor defects [N_0 in rows (7) and (8) of Table IV] and relatively large amounts of dissolved O_2 (Table I), it appears that new x-ray-created PROHC defects are not preferentially formed at pre-existing PROHC or O_2 sites, at the x-ray doses presently employed. Others have argued that the PROHC precursor may be an oxygen vacancy near an O_2 molecule.[64,81]

D. Trends in rates of creation versus activation

At high doses [≥ 80 Mrad (SiO_2)] all of the pre-existing E', H_W, or H_D precursor defects have been activated, so that any observed increase in spin count is linear in dose and is entirely due to creation.

At low doses [$\ll 5$ Mrad (SiO_2)] the increase in spin count is predicted to be essentially linear, but it generally consists of both a creation and an activation component. Figure 12(a) suggests that x-ray creation of E' centers dominates over activation at low dose as elsewhere. Table IV shows that for $T_F = 1350$ °C and $T_F = 700$ °C, $M_C/(M_C+M_A)$ is 0.71 and 0.93, with significant uncertainties. Averaging these two values we conclude that at low doses in Suprasil-1 at least 80% of the observed E' spins have been *created* and less than 20% have been activated. This numerical estimate is consistent with the impression given by Fig. 12(a).

Figure 12(b) suggests that activation of H_W spins dominates over creation at low dose, and Table IV bears this out: For $T_F = 1350$ and 700 °C, $M_A/(M_A+M_C)$ is 0.83 and 0.92, respectively. Averaging these two values we conclude that at low doses in Suprasil-1 at least 85% of the observed H_W spins have been *activated* and less than 15% have been created.

Figure 13(a) also reveals a dominance for activation over creation at low dose. Table IV shows that for $T_F = 1350$ and 1000 °C, $M_A/(M_A+M_C)$ is 0.85 (quite accurately) and 0.75, respectively. Averaging these we conclude that at low doses in Suprasil-$W1$ at least 80% of the observed E' spins have been *activated* and less than 20% have been created.

Finally, Fig. 13(b) suggests that activation of H_D spins strongly dominates over creation at low doses, and Table IV shows that $M_A/(M_A+M_C) \simeq 0.98$ for both $T_F = 1350$ and 1000 °C. We conclude, conservatively, that at low doses in Suprasil-$W1$ more than 95% of the observed H_D spins have been *activated* and less than 5% have been created.

These observations enable two different ways of studying creation and activation processes separately, without having to measure and analyze a complete N vs D curve. For H_W in Suprasil-1, as well as E' and H_D in Suprasil-$W1$, creation is studied alone by making differential measurements at high dose, while activation is emphasized by making measurements at low dose. Alternatively, for E' centers alone each process can be accessed at low dose: Creation is emphasized by low dose measurements in Suprasil-1, while activation is emphasized by low dose measurements in Suprasil-$W1$. Although two different sample types must be used, this latter method is quite convenient because large exposure times are not required.

VIII. POSSIBLE ASSOCIATIONS OF E', H_W, AND H_D DEFECTS WITH THE RAMAN-ACTIVE DEFECTS D_1 AND D_2

Two sharp lines, $D_1 = 495$ cm^{-1} and $D_2 = 606$ cm^{-1}, have been reported in the Raman spectra of v-SiO_2, and ascribed to defects in the network.[57] Subsequently, there has been much interest in ascertaining the origin of these defects,[25,58-63] and numerous broken bond (Refs. 16, 57, 58, 65, and 83–85), wrong bond (Refs. 25, 86, and 87) and other (Refs. 59–63, 68, and 88–90) models have been suggested. Among these are all three of the defect structures (Fig. 1) that are believed to account for the spin-resonance lines observed in the present study.

A. Evidence from N_0 that neither D_1 nor D_2 is the same defect as the precursor of either E', H_W, or H_D

We shall compare the [OH] and T_F dependencies of the number of pre-existing defects (N_0) with the [OH] and T_F dependencies of the number of Raman-active defects, and show that in general they do not correlate: That is, the precursor defects are *not* the same as the Raman-active defects, nor are they formed in constant intimate association with each other.

1. Evidence from the [OH] dependence of N_0

Raman studies[66] have shown that the concentrations of both D_1 and D_2 are quite independent of OH concentration from 2 to 1200 ppm (when the samples have been properly annealed to equilibrium at a common T_F). On the other hand, we found in Sec. VII A 2 (see the sixth column of Table IV) that the number of pre-existing E'

defects in a properly annealed dry sample is very much *greater* than in a wet sample. Thus neither D_1 nor D_2 is caused by the E' precursor defect, or by any other defect that might be produced in significant concentration in association with the precursor of E'. Since the E' center is confidently identified, and is not found prior to irradiation, we may further conclude that neither D_1 nor D_2 is a three-bonded silicon atom defect (nor is either due to any defect that might be formed in significant numbers in association with a three-bonded Si defect). *This is a simple and strong argument against the three-bonded Si atom models for D_1 or D_2.*

A similar argument can be made with respect to the precursors of the oxygen associated hole centers H_W and H_D. As indicated in Sec. VII A 2, H_W precursor defects disappear *almost completely* when a wet sample is replaced by a dry sample—and these pre-existing H_W defects are replaced by a preponderance of pre-existing H_D defects. Since the numbers of D_1 and D_2 defects remain constant with OH concentrations, neither of these can be associated with the H_W or H_D precursor defects. Assuming that the H_W and H_D center ESR lines are correctly identified with the NBOHC and PROHC structures shown in Fig. 1, we may further conclude that neither D_1 nor D_2 is a dangling oxygen atom, or a dangling peroxy bridge, or any defect that might be formed in significant concentration in association with these (as might happen with formation of valence alternation pairs[9,84,91–95]). *This is a simple and strong argument against models for D_1 or D_2 that involve dangling oxygen atoms or dangling peroxy bridges.*

The foregoing arguments concerning wet and dry materials do not depend on the fact that the x-ray photon spectrum used to irradiate the samples has the Cu-tube distribution shown in Fig. 3; this spectral distribution was the same for all samples, both wet and dry.

2. *Evidence from the T_F dependence of N_0*

One can construct additional *independent* arguments against associating D_1 or D_2 with certain of the spin-active defects using the observed changes with fictive temperature T_F, for a given [OH]. The relative strengths of D_1 and D_2 are given in the tenth and eleventh columns of Table IV. They were computed from the empirical expressions

$$A(D_1)=6.4\exp\left[\frac{-1624}{T_F}\right] \tag{8}$$

and

$$A(D_2)=48\exp\left[\frac{-4640}{T_F}\right]. \tag{9}$$

Compared to errors in the present measurements, the errors in values of A are negligible ($<5\%$). These expressions follow from the energies of thermal formation reported in Ref. 67: $E(D_1)=0.14\pm0.02$ eV and $E(D_2)=0.40\pm0.03$ eV.

The relevant comparisons are made in Table V. For example, the * in the second row indicates that the fractional change (0.43) in the concentration of Raman-active defect D_2 when going from T_H to T_L is incompatible with the corresponding fractional change (0.74) in the observed number of pre-existing H_W (NBOHC) precursor defects. Since the concentration of Raman-active D_2 did not change in the same proportion *within experimental errors* as the number of pre-existing H_W defects, we firmly conclude that the D_2 defects are not the same as the H_W precursor defects, nor are there any other defects produced in proportion to H_W precursors. This argument does not depend on the (unproven) assumption of Arrhenius behavior [Eq. (6)] for H_W, which assumption leads to the energy 0.06 eV given in the eighth column. The additional fact that $E(H_W)=0.06\pm0.07$ eV is incompatible with $E(D_2)=0.40\pm0.03$ eV is indicated by the † in the D_2 column [sixth column] of the second row in Table V.

In similar fashion, the * and † in the D_1 column [fifth column] of Table V indicate that D_1 and H_D precursors are not produced in compatible proportions (*) and their energies for thermal formation are also incompatible (†), within experimental errors. We thus firmly conclude from T_F dependencies that the D_1 defects are not the same as the H_D precursor defects, etc.

The fact that neither * nor † appear in any other entries in the fifth and sixth columns of Table V means that T_F *dependencies* do not rule out the other corresponding associations, e.g., D_2 with E' [first row, sixth column], etc. On the other hand, all other such associations are ruled out by the study of OH dependencies presented in Sec. VIII A 1.

Our proofs that neither D_1 nor D_2 is any one of the four point defect structures AOVEC, TBSEC, NBOHC, or PROHC (in their pre-existing precursor or spin-activated form) is consistent with Galeener's original assignment[5,60] of D_1 and D_2 to highly regular rings of Si-O bonds containing four and three Si atoms, respectively.[59–63,96] These very small rings are not *point* defects, but are *highly localized* elements of highly regular intermediate range order.[97,98]

The arguments in the first part of Sec. VIII A 1 not only show that the pre-existing precursor defects are not the same as the Raman-active defects, but that the pre-existing precursor defects are not formed in constant intimate association with the Raman-active defects. For example, formation of a nearby E' precursor with every D_1 ring, or pair of D_1 rings, etc., is ruled out.

B. Evidence from M_C that neither D_1 nor D_2 is a highly preferential site for x-ray formation of either E', H_W, or H_D

It has been suggested[99] that in sol-gel formed v-SiO_2 the Raman-active "ring defects" D_1 and D_2 may be highly preferred sites for the formation of the spin-active defects represented by the E', H_W, and H_D ESR lines. If this is true for the x-ray induction of a given point defect in our samples of bulk-formed v-SiO_2, then the creation rate M_C for that point defect should change in proportion to changes in the concentration of either D_1 or D_2, given by $A(D_1)$ or $A(D_2)$ [expressions (8) or (9)]. Suppose, for example, that D_2 defects are the *only* sites for

x-ray formation of E' centers in our materials. Then a doubling of the concentration of D_2 structures will produce twice as many newly created E' spins *per unit* of dose, i.e., M_C will be doubled.

We shall now compare the [OH] and T_F dependencies of the rate of creation of new spin-active defects (M_C) with the [OH] and T_F dependencies of the number of Raman-active defects, and show that in general they do not correlate: That is, the spin-active defects are *not* preferentially formed at the Raman-active structures when our samples are bombarded with x rays.

1. *Evidence from the [OH] dependence of M_C*

We noted earlier from Ref. 66 that the concentrations of both D_1 and D_2 are quite independent of [OH] from 2 to 1200 ppm, in samples with the same T_F. On the other hand, we found in Sec. VII C 2 (see the seventh column of Table IV) that M_C is *significantly* smaller in dry Suprasil-$W1$ than in wet Suprasil-1, both at $T_F=1350\,^\circ$C and at $T_F=700\,^\circ$C. We therefore conclude from the [OH] dependence of M_C that neither D_1 nor D_2 is the sole site for formation of E' centers under x-ray bombardment in our samples.

When [OH] is increased from <2 to 1200 ppm, the numbers of D_1 and D_2 are unchanged and the number of "normal" network sites (Si atoms, O atoms) is reduced by at most 1%; nevertheless, M_C is increased by at least 30%. This means that the observed dependence of M_C on [OH] {or [Cl], or [O_2]} is not due to a change in the number of x-ray interaction sites, but rather a change in the fraction of such interactions which result in a stable E' defect. Kerwin and Galeener[100] have recently shown that most of the observed spins are due to damage by the energetic electrons ejected from Si and O atoms by x-ray absorption. Presumably, increase in M_C with increasing [OH] has to do with an increasing ability of those energetic electrons to result in stable E' centers.

It is clear that our results do not *a priori* rule out the possibility that D_1 and/or D_2 are only slightly preferential sites. This is because the maximum available concentrations of D_1 or D_2 comprise at most about 1% of the atoms in the sample. We therefore say that [OH] dependencies of M_C demonstrate that neither D_1 nor D_2 is the sole site, or a "highly preferential" site, for creation of E' centers under x-ray bombardment of v-SiO_2. By highly preferential, we mean sufficiently preferential that, in spite of their small concentrations, the changes in the numbers of D_1 or D_2 would show a measurable influence on the rates of E' creation.

The [OH] dependencies of M_C for H_W and H_D are unknown. For example, when we go from Suprasil-1 to Suprasil-$W1$ in Table IV, the concentration of H_W goes to zero (unmeasurably small) so that the M_C for H_W in Suprasil-$W1$ is unmeasured, and we cannot even say whether it increases or decreases. This means that we cannot use *[OH] dependencies* of M_C to comment about D_1 or D_2 as sole sites for creation of H_W or H_D centers under x-ray bombardment.

2. *Evidence from the T_F dependence of M_C*

Additional conclusions can be drawn from the T_F dependence of M_C, as indicated in Table VI. Here, the * and † have the same utility as described in Sec. VIII A 2. The * indicate that changes in M_C with fictive temperature for E' and H_W in Suprasil-1 and for E' in Suprasil-$W1$ do not correlate with the changes in concentration A of D_1 or D_2 defects. The † show that the apparent energies of formation E for these defects are incompatible with the energies $E(D_1)$ and $E(D_2)$. We conclude from Table VI that neither D_1 nor D_2 is a sole site, or highly preferential site, for creation of E' or H_W centers under x-ray bombardment of v-SiO_2.

The information in Table VI does not allow us to draw a similar conclusion regarding H_D. If we accept the aforementioned regular ring assignments for D_1 and D_2, and the assignments of E', H_W, and H_D shown in Fig. 1, then we may argue as follows. Since neither D_1 nor D_2 is a highly preferential site for x-ray creation of a TBSEC, AOVEC, or NBOHC, it seems even less likely that D_1 or D_2 would be a highly preferential site for x-ray creation of the PROHC. The PROHC requires locally excess oxygen, and there is no obvious reason that regular four

TABLE VI. Fictive temperature-dependent properties of the rate of creation M_C of new defects by x-ray bombardment, derived from data in the indicated rows of Table IV [e.g., (1) and (2)]. T_L and T_H are the lower and higher fictive temperatures for each spin type, given in Table IV. The ratio $M_C(T_L)/M_C(T_H)$ for each spin-active defect is to be compared with the ratio for the number of Raman-active "defects" in the fifth and sixth columns. The nominal energies of thermal formation E for each defect are calculated using Eq. (7) and given in the eighth column, with the error determined range indicated by minimum and maximum values given in the seventh columns. In the fifth and sixth columns, * indicates incompatibility with the entry in the fourth column, while † denotes incompatibility with the seventh–ninth columns.

	(1)	(2)	(3)	(4)	(5)	(6)	(7)	(8)	(9)
Rows, Table IV	Sample	Spin type	Assigned defect structure	$M_C(T_L)/M_C(T_H)$	$A(T_L)/A(T_H)$ D_1	$A(T_L)/A(T_H)$ D_2	E (eV) Min	E (eV) Nom	E (eV) Max
(1) and (2)	Suprasil-1	E'	AOVEC	0.74±0.06	0.50*†	0.14*†	0.004	0.006	0.009
(3) and (4)		H_W	NBOHC	0.31±0.09	0.75*†	0.43*†	0.17	0.24	0.33
(5) and (6)	Suprasil-$W1$	E'	AOVEC	0.80±0.29	0.50*	0.14*†	−0.07	0.12	0.39
(7) and (8)		H_D	PROHC	0.50±0.53	0.75	0.43	−0.56	0.35	1.44

rings or three rings would provide this. We therefore think it likely that neither D_1 nor D_2 is a sole site, or highly preferential site, for creation of H_D centers under x-ray bombardment of v-SiO_2.

IX. RELATIVE RADIATION HARDNESS

Trends in Table IV also reveal strategies for improving the radiation hardness of v-SiO_2, where we associate "hardness" with reduced values of $N_T(D)=N_O+M_C D$, the total number of defect sites of a given type after dose D. $N_T(D)$ is therefore the maximum possible number of charges that can be trapped at that type of site.

Table IV shows that both N_O and M_C are reduced when T_F is lowered. A given material is thus made more radiation hard for all three traps at all exposures by annealing it to an equilibrium structure at the lowest practicable temperature T_F.

Achievement of enhanced radiation hardening by raising or lowering [OH] is also predicted, but the desired direction depends on the type of trap and the anticipated level of exposure. For example, consider the E' centers, whose pre-existing precursor number is much smaller in wet material than dry, but whose rate of creation by x rays is larger. The resultant $N_T(D)$ for our wet and dry material with $T_F=1350\,°C$ cross over at $D\simeq 220$ Mrad (SiO_2). While wet material is more rad-hard for electron traps below this dose, dry material is superior above it. For hole traps, dry material with $T_F=1350\,°C$ is harder above $D\cong 260$ Mrad.

X. SUPPORT FOR PUBLISHED ASSIGNMENTS

Various trends to be found in Table IV support the existing assignments of the ESR lines E', H_W, and H_D to the structures depicted in Figs. 1(a), 1(b), and 1(c), respectively.

For example, the N_0 in Table IV reveals that unirradiated wet Suprasil-1 material contains far fewer pre-existing E' center precursors than unirradiated dry Suprasil-$W1$ material. This important observation is consistent with the structure pictured in Fig. 1(a) and the intuitive notion that a plentitude of $-$OH units would convert most of the oxygen vacancy sites (the E' precursors) to pairs of fully bonded $\equiv$Si-OH sites, which are not E' precursors. The observation is also consistent with isolated TBSEC sites as defined in Sec. I.

Regarding newly created sites, we can see from the M_C in Table IV that for $T_F=1350\,°C$ x rays create new spins more easily in the order H_D, H_W, E', with E' the easiest (highest M_C). This sequence for the ease of creation of spins is consistent with the structural assignments in Fig. 1 as follows. Consider first the NBOHC structure in Fig. 1(b); this can be made merely by breaking one Si-O bond in a Si-O-Si bridge, producing both a NBOHC and a TBSEC. When spatially separated, as in the Griscom version of the Devine and Arndt model of Sec. I, these structures, $\equiv$Si-O and Si$\equiv$, will give rise to equal numbers of H_W and E' spins, respectively. Sometimes, however, both Si-O bonds in a Si-O-Si bridge will be cut, resulting in an AOVEC structure of the type shown in Fig. 1(a), and giving additional E' spins, but no H_W. If we assume that our created E' signals come from both three-bonded Si atoms and Fig. 1(a) structures, then irradiation will create more E' than H_W spins per x ray, as observed. On the other hand, it will be much easier to create a NBOHC than a PROHC, since in the latter case the x ray must (1) create a NBOHC, then *also* (2) liberate a nearby oxygen atom, and (3) allow it to combine with the NBOHC into a peroxy radical like that shown in Fig. 1(c). Thus we expect the creation of defect structures with x rays to become easier as we move leftward in Fig. 1. Using the published assignments,[25,39,58] this corresponds exactly to the order H_D, H_W, and E' observed for increasing M_C in Table IV.

XI. EVIDENCE THAT THE EFFICIENCIES OF CREATION AND ACTIVATION INCREASE WITH X-RAY PHOTON ENERGY

We found in Sec. III B that the E' and H_D signals were spatially distributed in the exposed samples in the form of a high density at the front surface, which drops rapidly through an apparent skin depth $\Delta_S\sim 40$ mm to a uniform background density δ_B, which extends throughout the 0.9-mm-thick samples. Table III shows that this background density is quite dependent on [OH] and T_F. Spatial distribution of the H_W signal is expected to be qualitatively similar. The large number of spins found near the back of the dry sample is surprisingly high, given that the back-surface dose is only 3% of that at the front surface (Sec. II B). This indicates that the efficiency with which spins are produced by x rays increases substantially with photon energy. Table III shows that δ_B is much higher for dry than wet material. Since dry material has far more pre-existing precursor defects than wet, and the x-ray-absorption profiles must be identical, we conclude that the large background values for E' and H_D spins in Table III must be largely due to spin activation of pre-existing defects in the dry material, rather than creation of new spin-active defects. *This conclusion suggests that the efficiency of activation increases more rapidly with photon energy than does the efficiency of creation.* Experiments verifying this prediction have been carried out.[101]

XII. SUMMARY AND CONCLUSIONS

We have carried out a systematic study of the electron spin-resonance signals E', H_W, and H_D, which are induced in v-SiO_2 by exposure to x rays from a Cu-target tube. Many conclusions were drawn, 24 of which are highlighted in this summary. We found that (1) the g values and linewidths of the spin signals are independent of x-ray exposure time t, hydroxyl content [OH] and sample fictive temperature T_F; (2) the *strengths* of the signals S depend in general on all three variables; and (3) the variations of S with exposure time t (shown in Figs. 6–9) in general are highly nonlinear for low t, but approach linear dependence for t greater than 20–30 h, up to $\sim$110 h.

Using appropriate calibration procedures, the data were converted from S to spin count N, and from t to (SiO_2) dose D, giving the points plotted in Figs. 12 and 13. To explain this data, we have further concluded that (4) two processes are at work concurrently; (5) in the first process, x rays progressively spin *activate* all pre-existing (unactivated) defects in the sample, thus accounting for the initial nonlinear region of the N vs D curves; (6) in the second process, x rays rupture bonds and *create* a continually increasing number of additional spin-active defects, thereby accounting for the linear portion of N vs D at higher doses [$D > 80$ Mrad (SiO_2)]; and (7) this activation plus creation model is expressed in the simple mathematical form of Eqs. (2)–(5), and fits well the various N vs D curves—producing parameters listed in Table IV. The most important parameters determined were as follows: N_O, a measure of the number of pre-existing precursor defects, M_C, a measure of the ability of the x-ray flux to *create* new centers and M_A, a measure of the rate with which a unit of the x-ray flux *activates* pre-existing precursors (of each kind).

Several trends were noted from the variations in these parameters. The most important are as follows: (8) In wet material there are very few pre-existing E' precursors, although there are substantial numbers of pre-existing H_W precursors; (9) in dry material there are substantial numbers of both pre-existing E' and H_D precursors; (10) in all cases for all defects the number of pre-existing defects *decreases* as T_F is substantially lowered; (11) the rate of *creation* of new E' centers is *greatest* in the wet material, although the number of pre-existing E' precursor defects is smallest; (12) in virtually all cases for all centers the rate of creation *decreases* as T_F is reduced, and as OH content is reduced; and (13) peroxy radical centers are very difficult to create with x-ray bombardment, as shown in Suprasil-$W1$.

These trends are obviously important in efforts to create the greatest number of spin-active or charge trapping defects in v-SiO_2 with a given dose of x rays or conversely to achieve the lowest number, the most radiation-hard material. We concluded that (14) both wet Suprasil-1 and dry Suprasil-$W1$ are more radiation hard when annealed to lower fictive temperatures T_F and (15) for *sufficiently high dose* radiation hardness is improved with lower [OH].

We made no effort to translate the trends in Table IV into clues about the microscopic processes of defect formation with x rays; this will be attempted after further experiments are carried out. However, we did exploit observed trends with OH concentration and T_F to conclude strongly that (16) the defects responsible for the E', H_W, and H_D spin signals or their precursor forms in v-SiO_2 are not the same as the defects responsible for the Raman-active lines D_1 and D_2. This means that D_1 and D_2 are not due to (or associated with) the three-bonded Si atom, the dangling oxygen, or the dangling peroxy bridge (which are identified in the literature as the sources of the three spin signals E', H_W, and H_D, respectively). We also concluded that (17) the pre-existing D_1 and D_2 (ring) structures are not sole or *highly* preferential sites for the formation of E', H_W or H_D spin-active defects as a result of x-ray bombardment. It follows more generally that (18) variations of dose curve parameters with T_F and [OH] as in Table IV can be used to test the possible role of E', H_W, and H_D defects in other phenomena. In addition to the present study of the D_1 and D_2 *Raman* lines, we are studying correlations between the T_F and [OH] behavior of spin signals and *luminescence* lines in v-SiO_2.[102]

It was also found that (19) trends in Table IV are consistent with the published assignments of the E', H_W, and H_D spin signals to the AOVEC, NBOHC, and PROHC structures, respectively, as defined in Fig. 1.

Finally, (20) our ability to separate creation from activation enables rationalization of the dose dependence, and study of each process separately. For example, (21) at low doses, creation dominates in wet Suprasil-1 and activation in dry Suprasil-$W1$; (22) at high doses the slope of the linear increase is due to creation alone in either kind of sample; and (23) studies of the photon energy dependence of each process under low dose circumstances[101] provides strong support for the present creation plus activation interpretation of the nonlinearity of x-ray dose curves in the dose ranges studied.

Our continuing work involves the use of nominally monochromatic x rays for studies of dose dependence, depth profiles, and the photon energy dependence of creation and of activation. We are also looking at significantly higher doses of x rays as well as the higher photon energies provided by γ rays. One goal is to better understand the microscopic nature of the creation and activation processes.

In general, we conclude that (24) quantitative study of the number of spins induced in glasses by x irradiation requires firm knowledge of the functional dependence of spin signal strength on the dose of nominally monoenergetic x rays. Our future experiments will concentrate on using narrow bands of photon energy as the inducing agent.

ACKNOWLEDGMENTS

The authors are deeply grateful to Dr. D. K. Biegelsen of Xerox PARC for instructing us in the use of his ESR spectrometer and for his friendly sharing of time on the instrument. We are also grateful to the United States Navy Office of Naval Research for partial support of the work under Contract No. N00014-91-J-1607 (G. B. Wright). F. L. G. is indebted to the Cavendish Laboratory of Cambridge University and to Dr. W. A. Phillips for their generous provision of resources during the writing and preparation of a first draft of the manuscript.

APPENDIX

After preparation of the first draft of this manuscript, the authors were made aware of an excellent review article by Friebele and Griscom.[103] While that review cites no work on the dose dependence of x-ray-induced ESR signals, it does cite early optical work,[104–106] which is

relevant to our subject. For example, Arnold and Compton[104] reported optical absorption coefficients for two defect absorption lines in v-SiO_2 that increased with MeV electron dose rather like our Figs. 12 and 13. They speculated that the two-stage form of the curves might represent a fast initial rise due to "trapping of electrons or holes at defects already present, while the later, nearly linear, portion of the growth curves may correspond to creation of the defects." Palma and Gagosz[106] fitted similar MeV electron irradiation optical data with expressions like Eqs. (2)–(5), but also included a *thermal* annealing term that is needed for high-flux electron irradiations at high temperatures, but not needed in our experiments. We also saw no evidence that our spin signals were changing with time after the x-ray bombardment, although *small* room temperature thermally induced changes might have been masked by the fact that the successive irradiations and ESR measurements were all made as contiguously in time as possible. In a single long-term check, one sample showed no change in E' spin count ($\pm 5\%$) when remeasured about six months after final exposure. Unfortunately most of the samples were subsequently destroyed in depth profiling, as described in Sec. III B.

As we have demonstrated elsewhere[100] the majority of the spins we measure are the result of *electron* damage, rather than relaxations of each ionized site formed by the initial photoabsorption of an x ray. Our measurements reveal very little about the low-energy mechanism (or mechanisms) by which those electrons finally produce stable centers. Nevertheless, the results are consistent with the work of Tsai and Griscom[107] who used 6.4-eV-excimer laser light to obtain direct evidence for the creation of oxygen vacancy and/or interstitial pairs in SiO_2 glasses by an excitonic mechanism. It is not unreasonable to suppose that the high-energy ejected electrons produced in our irradiations utilize $e^- - e^-$ scattering to give smaller amounts of energy to numerous other electrons. Some of these low-energy electron excitations would comprise excitons like those invoked in the models of Tsai and co-workers for formation of PROHC (Ref. 107) and E' (Refs. 107 and 108) centers.

Some other authors have recently reported nonlinear spin count versus dose curves and fit them with power laws of the form $N(D) \simeq D^n$. For example, Griscom[49] observed E' spin count versus x-ray dose at 77°K from 0.01 to 6 Mrad. His data were fit with $n \simeq 0.7$ for dry Suprasil-$W1$ and $n \simeq 0.88$ for wet Suprasil-1. All of Griscom's doses were below the minimum nonzero dose administered in our experiments, typically $\simeq 42$ Mrad (SiO_2). Because of his low temperatures (77° K) and his lower doses (≤ 6 Mrad) Griscom's data cannot be directly compared with ours. Nevertheless, it is easily seen from Figs. 12 and 13 that our model predicts some nonlinearity due to activation below 6 Mrad—and this nonlinearity would be qualitatively consistent with the sublinear behavior reported by Griscom. We are carrying out new experiments in this low dose regime.

In another example, Devine and Arndt[47] studied $N(D)$ for 1.25 MeV ^{60}Co γ-ray doses from about 0.1 to 10^7 Mrad. At lower doses ($0.1 \leq D \leq 10^2$ Mrad) they report n values of 0.58 and 0.77 for E' centers in Suprasil-$W1$ and Suprasil-1, respectively, and 0.25 for NBOHC. These (sublinear) n for E' centers are in rough agreement with those reported by Griscom and given in the previous paragraph. At higher doses ($10^4 \leq D \leq 10^7$ Mrad) the Devine and Arndt data are fit by different, typically higher and more linear values of n.

Although power-law fits were provided by Devine and Arndt, their data up to ~ 10 Mrad of γ irradiation look exactly like ours up to ~ 180 Mrad of x rays. *Thus, their data could have been fit well by our Eqs. (2)–(5), for γ-ray doses up to at least 10 Mrad.* This has been discussed in detail elsewhere by Galeener[109] who concludes that γ rays must be relatively more efficient in activation, per unit of dose, than are x rays. This might be expected from the work of Kerwin and Galeener[101] who showed in the 5–18-keV range that activation increases much more rapidly with photon energy than creation. As noted in Ref. 101, we strongly believe that one must not assume that equal doses of γ and x rays (in rads) give equal numbers of defect spins in v-SiO_2, nor do they give equivalent percentages of created and activated spins. Work is underway in our laboratory to obtain $N(D)$ at much higher *x-ray* doses, in order to compare with the γ-ray results of Devine and Arndt.[47]

[1] D. L. Griscom, in *Glass: Science and Technology,* edited by D. R. Uhlmann and N. J. Kreidl (Academic, Boston, 1990), Vol. 4B, p. 151ff.

[2] D. L. Griscom, J. Non-Cryst. Solids **40**, 211 (1980).

[3] D. L. Griscom, J. Non-Cryst. Solids **31**, 241 (1978).

[4] D. L. Griscom, in *The Physics of SiO_2 and its Interfaces,* edited by S. T. Pantelides (Pergamon, New York, 1978), p. 232.

[5] D. L. Griscom, in *Defects and Their Structure in Nonmetallic Solids,* edited by B. Henderson and A. E. Hughes (Plenum, New York, 1976), p. 323.

[6] D. L. Griscom, J. Non-Cryst. Solids **13**, 251 (1973/74).

[7] J. Wong and C. A. Angell, *Glass Structure by Spectroscopy* (Marcel Dekker, New York, 1976).

[8] D. L. Griscom, J. Non-Cryst. Solids **24**, 155 (1977).

[9] J. Robertson, Adv. Phys. **32**, 361 (1983).

[10] E. P. O'Reilly and J. Robertson, Phys. Rev. B **27**, 3780 (1983).

[11] R. A. Weeks, in *Interaction of Radiation with Solids,* edited by A. Bishay (Plenum, New York, 1967), p. 55.

[12] R. H. Doremus, *Glass Science* (Wiley, New York, 1973), p. 229.

[13] R. V. Adams and R. W. Douglas, J. Soc. Glass Technol. **43**, 147 (1959).

[14] G. H. A. M. van der Steen and E. Papanikolau, Phillips Res. Rep. **30**, 192 (1975).

[15] G. E. Walrafen, J. Chem. Phys. **62**, 297 (1975).

[16] R. H. Stolen and G. E. Walrafen, J. Chem. Phys. **64**, 2623 (1976).

[17] G. E. Walrafen and S. R. Samanta, J. Chem. Phys. **69**, 493 (1978).

[18] J. Stone and G. E. Walrafen, J. Chem. Phys. **76**, 1712 (1982).

[19] F. L. Galeener and R. H. Geils, in *The Structure of Non-Crystalline Materials,* edited by P. H. Gaskell (Taylor and

Francis, London, 1977), p. 223.
[20]F. L. Galeener and J. C. Mikkelsen, Jr., Appl. Phys. Lett. **38**, 336 (1981).
[21]J. C. Mikkelsen, Jr., F. L. Galeener, and W. J. Mosby, J. Electron. Mater. **10**, 631 (1981).
[22]R. A. Weeks, J. Appl. Phys. **27**, 1376 (1956).
[23]R. A. Weeks and C. M. Nelson, J. Appl. Phys. **31**, 1555 (1960).
[24]R. H. Silsbee, J. Appl. Phys. **32**, 1459 (1961).
[25]E. J. Friebele, D. L. Griscom, M. Stapelbroek, and R. A. Weeks, Phys. Rev. Lett. **42**, 1346 (1979).
[26]R. A. B. Devine and A. Golanski, J. Appl. Phys. **54**, 3833 (1983).
[27]R. A. B. Devine and M. H. Debroux, J. Appl. Phys. **54**, 4197 (1983).
[28]R. A. Weeks and M. Abraham, J. Chem. Phys. **42**, 68 (1965).
[29]K. L. Brower, Phys. Rev. Lett. **41**, 879 (1978).
[30]K. L. Brower, Phys. Rev. B **20**, 1799 (1979).
[31]R. A. Weeks and E. Lell, J. Appl. Phys. **35**, 1932 (1964).
[32]G. H. Sigel, Jr., E. J. Friebele, R. J. Ginther, and D. L. Griscom, IEEE Trans. Nucl. Sci. **NS-21**, 56 (1974).
[33]C. M. Nelson and R. A. Weeks, J. Am. Ceram. Soc. **43**, 396 (1960).
[34]R. A. Weeks and C. M. Nelson, J. Am. Ceram. Soc. **43**, 399 (1960).
[35]E. J. Friebele, D. L. Griscom, and G. H. Sigel, Jr., in *The Physics of Non-Crystalline Solids,* edited by G. H. Frischat (Trans. Tech., Adermannsdorf, Switzerland, 1977), p. 154.
[36]D. L. Griscom, Phys. Rev. B **20**, 1823 (1979).
[37]J. Vitko, Jr., J. Appl. Phys. **49**, 5530 (1978).
[38]M. Stapelbroek and D. L. Griscom, in *The Physics of SiO_2 and its Interfaces,* edited by S. T. Pantelides (Pergamon, New York, 1978), p. 263.
[39]M. Stapelbroek, D. L. Griscom, E. J. Friebele, and G. H. Sigel, Jr., J. Non-Cryst. Solids **32**, 313 (1979).
[40]K. L. Brown, P. M. Lenahan, and P. V. Dressendorfer, Appl. Phys. Lett. **41**, 251 (1982).
[41]D. L. Griscom, E. J. Friebele, K. J. Long, and J. W. Fleming, J. Appl. Phys. **54**, 3743 (1983).
[42]P. M. Lenahan and P. V. Dressendorfer, J. Appl. Phys. **55**, 3495 (1984).
[43]R. A. B. Devine and J.-M. Francou, Phys. Rev. B **41**, 12 882 (1990).
[44]R. A. B. Devine and J. Arndt, Phys. Rev. B **39**, 5132 (1989).
[45]F. J. Feigl and J. H. Anderson, J. Phys. Chem. Solids **31**, 575 (1970).
[46]V. S. Grunin and V. A. Ioffe, J. Non-Cryst. Solids **6**, 163 (1971).
[47]D. L. Griscom, M. Stapelbroek, and E. J. Friebele, J. Chem. Phys. **78**, 1638 (1983).
[48]F. L. Galeener and J. C. Mikkelsen, Jr., in *Induced Defects in Insulators,* edited by R. Mazzoldi (Les Editions de Physique, Paris, 1985), p. 141.
[49]D. L. Griscom, Nucl. Instrum. Methods B **46**, 12 (1990).
[50]F. L. Galeener, D. B. Kerwin, A. J. Miller, and J. C. Mikkelsen, Jr., Solid State Commun. **82**, 271 (1992).
[51]T. W. Hickmott, J. Appl. Phys. **45**, 1050 (1974).
[52]J. J. Hauser, G. A. Pasteur, A. Staudinger, and R. S. Hutton, J. Non-Cryst. Solids **46**, 59 (1981).
[53]F. J. Feigl, W. B. Fowler, and K. L. Yip, Solid State Commun. **14**, 225 (1974).
[54]Heraeus-Amersil, 3473 Satellite Blvd., Duluth, GA 30136.
[55]D. L. Griscom, J. Ceram. Soc. Jpn. **99**, 923 (1991).
[56]F. L. Galeener, J. Non-Cryst. Solids **71**, 373 (1985).
[57]R. H. Stolen, J. T. Krause, and C. R. Kurkjian, Discuss. Faraday Soc. **50**, 103 (1970).
[58]J. B. Bates, R. W. Hendricks, and L. B. Shaffer, J. Chem. Phys. **61**, 4163 (1974).
[59]F. L. Galeener, J. Non-Cryst. Solids **49**, 53 (1982).
[60]F. L. Galeener, Solid State Commun. **44**, 1037 (1982).
[61]F. L. Galeener, in *The Structure of Non-Crystalline Materials 1982,* edited by P. H. Gaskell, J. M. Parker, and E. A. Davis (Taylor and Francis, London, 1983), p. 337.
[62]J. C. Phillips, Solid State Phys. **37**, 93 (1982).
[63]F. L. Galeener and A. C. Wright, Solid State Commun. **57**, 677 (1986).
[64]R. L. Pfeffer, in *The Physics and Technology of Amorphous SiO_2,* edited by R. A. B. Devine (Plenum, New York, 1988), p. 181.
[65]F. L. Galeener, J. C. Mikkelsen, Jr., and N. M. Johnson, in *The Physics of SiO_2 and Its Interfaces* (Ref. 38), p. 284.
[66]J. C. Mikkelsen, Jr. and F. L. Galeener, J. Non-Cryst. Solids **37**, 71 (1980).
[67]A. E. Geissberger and F. L. Galeener, Phys. Rev. B **28**, 3266 (1983).
[68]F. L. Galeener and G. Lucovsky, Phys. Rev. Lett. **37**, 1474 (1976).
[69]F. L. Galeener and P. N. Sen, Phys. Rev. B **17**, 1928 (1978).
[70]R. M. Martin and F. L. Galeener, Phys. Rev. B **23**, 3071 (1981).
[71]See, e.g., B. D. Cullity, *Elements of X-Ray Diffraction* (Addison-Wesley, Reading, MA, 1956).
[72]A. F. Burr, in *CRC Handbook of Radiation Measurement and Protection,* edited by A. B. Broadsky (CRC Press, Boca Raton, 1978), p. 244ff.
[73]P. Kirkpatrick and L. Wiedmann, Phys. Rev. **67**, 321 (1945).
[74]R. Birch and M. Marshall, Phys. Med. Biol. **24**, 505 (1979).
[75]D. B. Brown and J. V. Gilfrich, J. Appl. Phys. **42**, 4044 (1971).
[76]R. W. Fink, R. C. Jopson, H. Mark, and C. D. Swift, Rev. Mod. Phys. **38**, 573 (1966).
[77]D. B. Brown and R. E. Oglivie, J. Appl. Phys. **37**, 4429 (1966).
[78]D. B. Brown, D. B. Wittry, and D. F. Kyser, J. Appl. Phys. **40**, 1627 (1969).
[79]A. R. Ruffa, Phys. Rev. Lett. **25**, 650 (1970).
[80]C. P. Poole, Jr., *Electron Spin Resonance* (Wiley, New York, 1983), p. 577.
[81]A. H. Edwards and W. B. Fowler, Phys. Rev. B **26**, 6649 (1982).
[82]J. H. Stathis and M. A. Kastner, Phys. Rev. B **29**, 7079 (1984).
[83]G. N. Greaves, J. Non-Cryst. Solids **32**, 295 (1979).
[84]G. Lucovsky, Philos. Mag. **39**, 513 (1979).
[85]R. B. Laughlin, J. D. Joannopoulos, C. A. Murray, K. Hartnett, and T. J. Greytak, Phys. Rev. Lett. **40**, 461 (1978).
[86]C. A. Murray and T. J. Greytak, J. Chem. Phys. **71**, 3355 (1979).
[87]A. R. Silin and P. J. Bray, Bull. Am. Phys. Soc. **26**, 218 (1981).
[88]S. K. Sharma, J. F. Mammone, and M. Nicol, Nature (London) **292**, 140 (1981).
[89]A. G. Revesz and G. E. Walrafen, in *The Structure of Non-Crystalline Materials 1982,* edited by P. H. Gaskell, J. M. Parker and E. A. Davis (Taylor and Francis, London, 1983), p. 360.
[90]S. W. Barber, in *The Physics of SiO_2 and Its Interfaces* (Ref. 38), p. 139.
[91]G. Lucovsky, Philos. Mag. B **39**, 531 (1979).
[92]R. A. Street and G. Lucovsky, Solid State Commun. **31**, 289 (1979).
[93]G. Lucovsky, Philos. Mag. B **41**, 457 (1980).
[94]G. Lucovsky, J. Non-Cryst. Solids **35–36**, 825 (1980).

[95]K. Shimakawa and A. Kondo, Phys. Rev. B **27**, 1136 (1983).
[96]F. L. Galeener, R. A. Barrio, E. Martinez, and R. J. Elliott, Phys. Rev. Lett. **53**, 2429 (1984).
[97]F. L. Galeener, J. Non-Cryst. Solids **123**, 182 (1990).
[98]F. L. Galeener, in *Disorder in Condensed Matter Physics,* edited by J. Blackman and J. Taguena (Oxford University Press, Oxford, 1991), p. 45.
[99]W. L. Warren, P. M. Lenahan, and C. J. Brinker, Solid State Commun. **79**, 137 (1991).
[100]D. B. Kerwin and F. L. Galeener, Appl. Phys. Lett. **59**, 2959 (1991).
[101]D. B. Kerwin and F. L. Galeener, Phys. Rev. Lett. **68**, 3208 (1992).
[102]D. B. Kerwin and F. L. Galeener (unpublished).
[103]E. J. Friebele and D. L. Griscom, in *Treatises on Materials Science and Technology,* edited by M. Tomozawa and R. H. Doremus (Academic, New York, 1979), Vol. 17, p. 257.
[104]G. W. Arnold and W. D. Compton, Phys. Rev. **116**, 802 (1959).
[105]W. D. Compton and G. W. Arnold, Discuss. Faraday Soc. **31**, 130 (1961).
[106]G. E. Palma and R. M. Gagosz, J. Phys. Chem. Solids **33**, 177 (1972).
[107]T. E. Tsai and D. L. Griscom, Phys. Rev. Lett. **67**, 2517 (1991).
[108]T. E. Tsai, D. L. Griscom, and E. J. Friebele, Phys. Rev. Lett. **61**, 444 (1988).
[109]F. L. Galeener, J. Non-Cryst. Solids **149**, 27 (1992).